ALP-induced polarization effects on photons from blazars

Giorgio Galanti[*]
INAF, Istituto di Astrofisica Spaziale e Fisica Cosmica di Milano, Via Alfonso Corti 12, I—20133 Milano, Italy

Marco Roncadelli[†]
INFN, Sezione di Pavia, Via Agostino Bassi 6, I—27100 Pavia, Italy and INAF, Osservatorio Astronomico di Brera, Via Emilio Bianchi 46, I—23807 Merate, Italy

Fabrizio Tavecchio[‡]
INAF, Osservatorio Astronomico di Brera, Via Emilio Bianchi 46, I—23807 Merate, Italy

(Received 24 May 2023; accepted 14 September 2023; published 12 October 2023)

Axionlike particles (ALPs), which are very light neutral spin zero elusive particles primarily interacting with two photons and predicted by superstring and superbrane theories, have come to help by solving two distinct problems about blazars (a type of active galactic nuclei), thus providing two hints at the existence of ALPs themselves. In the presence of an external magnetic field, ALPs produce (i) photon-ALP oscillations and (ii) the change of the polarization state of photons. The former effect has many consequences in the astrophysical contest, such as the modification of the transparency of the Universe and the alteration of the astrophysical spectra. We address here the latter effect by analyzing how the photon degree of linear polarization and the polarization angle get modified by the photon-ALP interaction in the case where photons are generated at the jet base of some BL Lacs (a blazar class): OJ 287, BL Lacertae, Markarian 501 and 1ES 0229 + 200, by considering both a leptonic and hadronic emission mechanism. We show that OJ 287 and BL Lacertae are good observational targets for ALP studies both in the x-ray band with IXPE (already operative) and with the proposed eXTP, XL-Calibur, NGXP and XPP missions, and in the high-energy range with the COSI, e-ASTROGAM and AMEGO missions, while 1ES 0229 + 200 represents a strong candidate in the x-ray band only. Since these blazars show a very high final photon degree of linear polarization—which cannot be explained by conventional physics—such a possible detection would represent an additional hint at the ALP existence. Instead, Markarian 501 does not appear as a good target for these studies. We conclude that all these observatories can give us additional fundamental information about ALP physics.

DOI: 10.1103/PhysRevD.108.083017

I. INTRODUCTION

Several extensions of the standard model of particle physics, such as the superstring and superbrane theories [1–10], invariably predict the existence of axionlike particles (ALPs, see e.g. [11,12] for reviews). ALPs are very light neutral pseudoscalar bosons and are nowadays considered among the best candidates for the dark matter [13–17]. ALPs are a generalization of the axion, namely the pseudo-Goldsone boson arising from the breakdown of the global Peccei-Quinn symmetry $\mathrm{U}(1)_{\mathrm{PQ}}$ proposed as a solution of the strong CP problem (see e.g. [18–21] for reviews). However, ALPs differ from the original axion in two main respects: (i) the ALP mass m_a and the ALP-to-two-photon coupling $g_{a\gamma\gamma}$ are uncorrelated quantities while they are linked in the case of the axion, and (ii) ALPs primarily interact with two photons, while other interactions with fermions and gluons—which are instead fundamental in the case of the axion—are subdominant. When an external magnetic field is present, two effects are produced: (i) photon-ALP oscillations [22,23] and (ii) the change of the polarization state of photons [22,23].

ALP detection is made difficult by their very faint interaction with photons over distances attainable in laboratory experiments. Instead, since the astrophysical environment is not affected by this limitation, it offers the best opportunity to study ALP physics especially in the high-energy (HE) and very-high-energy (VHE) bands, where the former effect, i.e. photon-ALP oscillation, leads to many consequences (see e.g. [24–26]). At the same time, VHE astrophysics presents a few challenges, whose solutions have repeatedly invoked the existence of ALPs. In particular, two

[*]gam.galanti@gmail.com
[†]marcoroncadelli@gmail.com
[‡]fabrizio.tavecchio@inaf.it

hints at the ALP existence arise from blazars, which are a class of active galactic nuclei (AGN). Specifically, ALPs naturally explain why flat spectrum radio quasars (a blazar subclass) are observed up to 400 GeV, in spite of the fact that conventional physics prevents any emission above 30 GeV [27]—which represents a first hint at the existence of an ALP. In addition, an ALP with the same properties solves the anomalous redshift-dependence of the *emitted* spectra of BL Lacs (a blazar subclass) [28]: this represents a second hint. The photon-ALP interaction is also responsible for the alteration of the photon cosmic transparency (see e.g. [29,30]) and gives rise to an oscillatory behavior in observed spectra [31–36]. The detection of the gamma-ray burst GRB 221009A up to 18 TeV by LHAASO [37] and even at 251 TeV by Carpet-2 [38] strongly suggests the existence of an ALP with the *same* properties as in the previous two hints [39].

Also the latter above-mentioned ALP effect—namely the change of the photon polarization state—has sizable and detectable consequences. In particular, the polarization of photons from gamma-ray bursts has been investigated in [40], while other studies cover different topics concerning several astrophysical sources [41–46]. In addition, the photon-ALP interaction can be employed to measure *emitted* photon polarization [47]. Very recently, ALP-induced polarization effects have been analyzed when photons are generated in the central region of galaxy clusters or in the blazar jet [48]. In particular, the Perseus and Coma clusters have been identified as solid targets for studies concerning ALP effects on photon polarization [49]. Because of the very recent interest on photon polarization—as shown by the launch or proposal of new observatories in the x-ray band like IXPE [50], eXTP [51], XL-Calibur [52], NGXP [53] and XPP [54] and in the HE range such as COSI [55], e-ASTROGAM [56,57] and AMEGO [58]—in this paper we address peculiar BL Lacs in order to find out which are the best observational targets for ALP studies.

In particular, by closely following the analysis developed in [48], we investigate the photon-ALP beam propagation for photons emitted at the jet base of various BL Lacs: OJ 287, BL Lacertae, Markarian 501 and 1ES 0229 + 200. We compute—for each of them—the photon survival probability in the presence of the photon-ALP interaction $P_{\gamma\to\gamma}$, the corresponding final photon degree of linear polarization Π_L and polarization angle χ. By using the state-of-the-art knowledge concerning the crossed regions (blazar jet, host galaxy, extragalactic space, Milky Way) and physically consistent bounds on the photon-ALP system parameters, we conclude that ALPs induce sizable effects on the final photon polarization which is observable by present and planned missions [50–58]. In particular, OJ 287 and BL Lacertae appear as good observational targets both in the x-ray and in the HE band, 1ES 0229 + 200 in the x-ray range only, while Markarian 501 does not represent a good candidate for studies of ALP effects on photon polarization.

The paper is organized as follows. In Sec. II we introduce ALPs and their induced polarization effects, in Sec. III we cursorily describe the properties of the media crossed by the photon-ALP beam, in Sec. IV we present our results, while in Sec. V we draw our conclusions.

II. AXIONLIKE PARTICLES AND POLARIZATION EFFECTS

ALPs are very light neutral pseudoscalar bosons, whose primary interaction with two photons is governed by the Lagrangian,

$$\begin{aligned}\mathcal{L}_{\rm ALP} &= \frac{1}{2}\partial^\mu a \partial_\mu a - \frac{1}{2}m_a^2 a^2 - \frac{1}{4}g_{a\gamma\gamma}F_{\mu\nu}\tilde{F}^{\mu\nu}a \\ &= \frac{1}{2}\partial^\mu a \partial_\mu a - \frac{1}{2}m_a^2 a^2 + g_{a\gamma\gamma}\mathbf{E}\cdot\mathbf{B}\,a, \end{aligned} \tag{1}$$

where a is the ALP field, while $\mathbf{E}$ and $\mathbf{B}$ denote the electric and magnetic parts of the electromagnetic tensor $F_{\mu\nu}$, whose dual is represented by $\tilde{F}^{\mu\nu}$. In many VHE studies in addition to Eq. (1) also the Heisenberg-Euler-Weisskopf (HEW) effective Lagrangian,

$$\mathcal{L}_{\rm HEW} = \frac{2\alpha^2}{45m_e^4}[(\mathbf{E}^2-\mathbf{B}^2)^2 + 7(\mathbf{E}\cdot\mathbf{B})^2], \tag{2}$$

must be considered, where α is the fine-structure constant, while m_e is the electron mass [59–61]. Equation (2) describes the photon one-loop vacuum polarization. This effect can be relevant in the case of hadronic emission models for the very high central jet magnetic field (see also [34,62] and Sec. III). Because of the structure of the photon-ALP coupling in Eq. (1), the component $\mathbf{B}_T$ of $\mathbf{B}$ transverse to the photon momentum $\mathbf{k}$ turns out to be the only one relevant for the photon-ALP interaction. In Eq. (1), $\mathbf{E}$ is the electric field associated with a propagating photon. An additional effect to be taken into account is the photon dispersion on the cosmic microwave background (CMB) [63].

Many bounds on the ALP parameters (m_a, $g_{a\gamma\gamma}$) exist in the literature [64–75]; however, the most reliable one is that of CAST, arising from no-detection of ALPs from the Sun and reads $g_{a\gamma\gamma} < 0.66\times10^{-10}$ GeV^{-1} for $m_a < 0.02$ eV at the 2σ level [64].

We consider a photon-ALP beam of energy E exhibiting $\gamma \leftrightarrow a$ oscillations, and propagating along the y-direction in various magnetized media—blazar jet, host galaxy, extragalactic space, Milky Way—until it arrives to the Earth, where photons can be detected. Since in the present analysis $E \gg m_a$, the short-wavelength approximation [22] holds, and the propagation equation of an unpolarized photon-ALP beam described by $\mathcal{L}_{\rm ALP}$ in Eq. (1) reads

$$i\frac{d\rho(y)}{dy} = \rho(y)\mathcal{M}^{\dagger}(E,y) - \mathcal{M}(E,y)\rho(y), \tag{3}$$

where $\mathcal{M}(E,y)$ is the photon-ALP system mixing matrix accounting for the photon-ALP interaction strength, the ALP and the effective photon mass, the magnetization and absorption properties of the crossed media (for more details see [62]). In Eq. (3), $\rho(y)$ is the polarization density matrix of the photon-ALP system whose form is

$$\rho(y) = \begin{pmatrix} A_x(y) \\ A_z(y) \\ a(y) \end{pmatrix} \otimes \begin{pmatrix} A_x(y) & A_z(y) & a(y) \end{pmatrix}^*, \tag{4}$$

where $A_x(y)$ and $A_z(y)$ are the photon linear polarization amplitudes along the x and z axis, respectively and $a(y)$ is the ALP amplitude. Equation (3) can be solved by means of the *transfer matrix* of the photon-ALP system $\mathcal{U}(E;y,y_0)$ as

$$\rho(y) = \mathcal{U}(E;y,y_0)\rho_0\mathcal{U}^{\dagger}(E;y,y_0), \tag{5}$$

where ρ_0 is the density matrix at position y_0. The probability that a photon-ALP beam starting in the state ρ_0 at position y_0 is found at position y in the state ρ is

$$P_{\rho_0\to\rho}(E,y) = \mathrm{Tr}[\rho\mathcal{U}(E;y,y_0)\rho_0\mathcal{U}^{\dagger}(E;y,y_0)], \tag{6}$$

with $\mathrm{Tr}\rho_0 = \mathrm{Tr}\rho = 1$ [30].

Pure photon states polarized along the x and z directions are described by the matrices,

$$\rho_x = \begin{pmatrix} 1 & 0 & 0 \\ 0 & 0 & 0 \\ 0 & 0 & 0 \end{pmatrix}, \qquad \rho_z = \begin{pmatrix} 0 & 0 & 0 \\ 0 & 1 & 0 \\ 0 & 0 & 0 \end{pmatrix}, \tag{7}$$

respectively, the ALP state by

$$\rho_a = \begin{pmatrix} 0 & 0 & 0 \\ 0 & 0 & 0 \\ 0 & 0 & 1 \end{pmatrix}, \tag{8}$$

whereas

$$\rho_{\mathrm{unpol}} = \frac{1}{2}\begin{pmatrix} 1 & 0 & 0 \\ 0 & 1 & 0 \\ 0 & 0 & 0 \end{pmatrix}, \tag{9}$$

represents an unpolarized photon state. Partially polarized photons are characterized by a polarization density matrix with an intermediate functional expression between Eqs. (7) and (9).

The photonic part of the polarization density matrix of Eq. (4) derived from Eq. (5) is written in terms of the Stokes parameters as [76]

$$\rho_\gamma = \frac{1}{2}\begin{pmatrix} I+Q & U-iV \\ U+iV & I-Q \end{pmatrix}, \tag{10}$$

with the definition of the photon degree of *linear polarization* Π_L and of the *polarization angle* χ being [77]

$$\Pi_L \equiv \frac{(Q^2+U^2)^{1/2}}{I} = \frac{[(\rho_{11}-\rho_{22})^2 + (\rho_{12}+\rho_{21})^2]^{1/2}}{\rho_{11}+\rho_{22}}, \tag{11}$$

$$\chi \equiv \frac{1}{2}\arctan\left(\frac{U}{Q}\right) = \frac{1}{2}\arctan\left(\frac{\rho_{12}+\rho_{21}}{\rho_{11}-\rho_{22}}\right), \tag{12}$$

respectively, which are expressed in terms of the photon polarizaton density matrix elements ρ_{ij} with $i,j = 1,2$.

In order to define the different regimes of the photon-ALP beam propagation, we define the *low-energy threshold* E_L and the *high-energy threshold* E_H as [78]

$$E_L \equiv \frac{|m_a^2 - \omega_{\mathrm{pl}}^2|}{2g_{a\gamma\gamma}B_T}, \tag{13}$$

and

$$E_H \equiv g_{a\gamma\gamma}B_T\left[\frac{7\alpha}{90\pi}\left(\frac{B_T}{B_{\mathrm{cr}}}\right)^2 + \rho_{\mathrm{CMB}}\right]^{-1}, \tag{14}$$

respectively, where $\omega_{\mathrm{pl}} = (4\pi\alpha n_e/m_e)^{1/2}$ is the plasma frequency with n_e denoting the electron number density, $B_{\mathrm{cr}} \simeq 4.41\times10^{13}$ G is the critical magnetic field, and $\rho_{\mathrm{CMB}} = 0.522\times10^{-42}$ accounts for the photon dispersion on the cosmic microwave background (CMB) [63].

In the energy range $E_L \lesssim E \lesssim E_H$ the photon-ALP beam propagates in the *strong-mixing* regime, wherein the plasma contribution, the ALP mass term, the QED one-loop effect and the photon dispersion on the CMB are negligible. In such a situation the photon survival probability in the presence of the photon-ALP oscillations $P_{\gamma\to\gamma}$ is maximal and energy independent. Instead, for $E \lesssim E_L$ the plasma contribution and/or the ALP mass are dominant and the same is true for $E \gtrsim E_H$ concerning the QED one-loop effect and/or the photon dispersion on the CMB: in either case the photon-ALP beam propagates in the *weak-mixing* regime and $P_{\gamma\to\gamma}$ is energy-dependent and progressively vanishing.

In the following, we derive $P_{\gamma\to\gamma}$ and the corresponding Π_L and χ taking all the magnetization and absorption properties of the crossed media into account by using the state-of-the-art knowledge (see also [48,49] and Sec. III for more details).

We conclude this section by mentioning that a strict relationship between the *emitted* photon degree of linear polarization $\Pi_{L,0}$ and the photon survival probability $P_{\gamma\to\gamma}$ in the absence of photon absorption has been demonstrated

in [47]. In particular, we have $P_{\gamma\to\gamma} \geq (1-\Pi_{L,0})/2$. Among other things, the inequality derived in [47] represents a check for the correctness of our results. We have indeed made sure that $P_{\gamma\to\gamma}$ satisfies such a relation in all the following figures.

III. PHOTON-ALP BEAM PROPAGATION

In the following, we schematically illustrate the main properties of the astrophysical media crossed by the photon-ALP beam (blazar jet, host galaxy, extragalactic space, Milky Way), by underlining those which are more important for the photon-ALP system. For a complete description, we address the reader also to [48,49] and to the publications dealing with the particular topic cited below. Concerning the photon-ALP system parameters, we assume the benchmark values $g_{a\gamma\gamma} = 0.5\times 10^{-11}$ GeV^{-1} and the two ALP masses: (i) $m_a \lesssim 10^{-14}$ eV and (ii) $m_a = 10^{-10}$ eV. This choice allow us to meet the ALP bound by CAST [64].

A. Blazar

Blazars are a class of AGN, namely extragalactic supermassive black holes (SMBHs), which efficiently accrete matter from the surrounding. In such a situation, two collimated relativistic jets are emitted in opposite directions. When, just by chance, one of them turns out to be in the direction of the Earth, the AGN is called a blazar. In the following, we deal with a subclass of blazars called BL Lac objects (BL Lacs). BL Lacs are less powerful than the objects of the other class called flat spectrum radio quasars (FSRQs), and at variance with FSRQs lack strong optical emission lines and VHE absorption regions.

Photons are generated at the BL Lac emission region, which lies at a distance of about $y_{\rm em} = (10^{16}$–$10^{17})$ cm from the central SMBH. Then, photons can oscillate into ALPs in the magnetic field of the jet $\mathbf{B}^{\rm jet}$ until it ends at a distance of about 1 kpc. Here, the photon-ALP beam enters the host galaxy. Since we are far enough from the center, the toroidal part of $\mathbf{B}^{\rm jet}$—transverse to the jet axis [79–81]—is dominant, and its profile reads

$$B^{\rm jet}(y) = B_0^{\rm jet}\left(\frac{y_{\rm em}}{y}\right), \tag{15}$$

where $B_0^{\rm jet}$ represents the jet magnetic field strength at $y_{\rm em}$. The electron number density $n_e^{\rm jet}$ profile is given by

$$n_e^{\rm jet}(y) = n_{e,0}^{\rm jet}\left(\frac{y_{\rm em}}{y}\right)^2, \tag{16}$$

for the conical shape of the jet. In Eq. (16) $n_{e,0}^{\rm jet}$ is the jet electron number density at $y_{\rm em}$. Synchrotron self Compton (SSC) diagnostics applied to blazar spectra suggests to take $n_{e,0}^{\rm jet} = 5\times 10^4$ cm^{-3} [82].

In the following, we consider both a leptonic and a hadronic emission mechanism. In either case photons in the optical up to the x-ray band are generated by electron-synchrotron emission, while at higher energies the leptonic model gives rise to photons via inverse Compton scattering [83–85], whereas the hadronic mechanism produces higher energy photons by proton-synchrotron emission or photomeson production [86–88]. The values of $B_0^{\rm jet}$ and $y_{\rm em}$ are crucial for the photon-ALP system: the hadronic model requires higher values of $B_0^{\rm jet}$ and $y_{\rm em}$ as compared with the leptonic one. In addition, a higher initial degree of linear polarization $\Pi_{L,0}$ is predicted by hadronic models with respect to that expected in the leptonic scenario.

We compute the photon-ALP beam propagation in the jet comoving frame: thus, we must apply the transformation $E\to\gamma E$, where γ is the Lorentz factor, when passing to the fixed frames of the regions to be considered below. The analysis of the photon-ALP conversion and the calculation of the transfer matrix in the jet $\mathcal{U}_{\rm jet}$ is reported in [89].

The parameter values concerning $B_0^{\rm jet}$, $y_{\rm em}$, γ and $\Pi_{L,0}$ vary from leptonic to hadronic models, and also for the specific sources: we refer the reader to the subsequent subsections about the specific BL Lacs for more details.

B. Host galaxy

BL Lacs are commonly hosted by elliptical galaxies, which are characterized by a turbulent magnetic field $\mathbf{B}_{\rm host}$, which is usually described by means of a domainlike model. Typical values of the strength and of the coherence length of $\mathbf{B}_{\rm host}$ are $B_{\rm host}\simeq 5$ μG and $L_{\rm dom}^{\rm host}\simeq 150$ pc, respectively [90]. Photon-ALP oscillations are inefficient in this region because of the very high $\gamma\leftrightarrow a$ oscillation length when compared to $L_{\rm dom}^{\rm host}$ as shown in [27]. Therefore, the resulting transfer matrix in the host galaxy is $\mathcal{U}_{\rm host}\simeq 1$.

C. Galaxy cluster

All BL Lacs considered in this paper are located outside rich galaxy clusters. Here, we are thus considering an alternate scenario with respect to that explored in [48], where blazars were supposed to be hosted by rich galaxy clusters. The photon-ALP conversion is not efficient in the situation considered here: therefore, the cluster transfer matrix reads $\mathcal{U}_{\rm clu}\simeq 1$.

D. Extragalactic space

The extragalactic space is a region of high photon absorption in the VHE band because of the existence of the extragalactic background light (EBL) [91–94]. However, we are dealing with much lower energies in the present paper, and so the EBL absorption turns out to be negligible. Therefore, the photon-ALP interaction in this region modifies $P_{\gamma\to\gamma}$ and the corresponding Π_L and χ in a way which depends on the strength and morphology of the extragalactic magnetic field $\mathbf{B}_{\rm ext}$.

Unfortunately, $\mathbf{B}_{\rm ext}$ is currently poorly known: only the most recent bound 10^{-7} nG $\leq B_{\rm ext} \leq 1.7$ nG on the scale of $\mathcal{O}(1)$ Mpc exists [95–97]. As a matter of fact, $\mathbf{B}_{\rm ext}$ is commonly described by means of a domainlike model [98,99], wherein $\mathbf{B}_{\rm ext}$ changes discontinuously at the interface of two adjacent domains. We employ the new improved version of this model—described in [62]—which avoids such an unphysical behavior of the original proposal which produces inaccurate results. In the new model, $\mathbf{B}_{\rm ext}$ possesses a constant strength and orientation in the central part of each domain of size $L^{\rm ext}_{\rm dom}$, but smoothly and continuously connects to the orientation of $\mathbf{B}_{\rm ext}$ in the adjacent domains.

Since outflows from primeval galaxies predict rather high values of $B_{\rm ext}$ with $B_{\rm ext} = \mathcal{O}(1)$ nG for $L^{\rm ext}_{\rm dom} = \mathcal{O}(1)$ Mpc [100–103], we assume $B_{\rm ext} = 1$ nG for definiteness and $L^{\rm ext}_{\rm dom}$ randomly varying with a power-law distribution function $\propto (L^{\rm ext}_{\rm dom})^{-1.2}$ in the range (0.2–10) Mpc and with $\langle L^{\rm ext}_{\rm dom} \rangle = 2$ Mpc [62].

Following the procedure developed in [34,62], we compute the transfer matrix of the photon-ALP system in the extragalactic space $\mathcal{U}_{\rm ext}$.

E. Milky Way

There exist nowadays detailed maps of the Milky Way electron number density $n_e^{\rm MW}$ and magnetic field $\mathbf{B}_{\rm MW}$. In particular, we employ the model developed in [104] concerning $n_e^{\rm MW}$ and that by Jansson and Farrar [105–107] regarding $\mathbf{B}_{\rm MW}$. Although also the $\mathbf{B}_{\rm MW}$ model by Pshirkov *et al.* [108] is present in the literature and leads to similar results, we prefer that by Jansson and Farrar [105–107], since it turns out to be more complete, as it accurately describes also the Galactic halo component.

Although the regular component of $\mathbf{B}_{\rm MW}$ gives the maximal contribution to the photon-ALP interaction, we take into account also the turbulent part of $\mathbf{B}_{\rm MW}$ in the calculation of the photon-ALP conversion in the Milky Way.

The transfer matrix $\mathcal{U}_{\rm MW}$ of the photon-ALP system inside the Milky Way is evaluated by following the strategy developed in [35].

F. Overall photon-ALP beam propagation

By combining in the correct order the transfer matrices $\mathcal{U}_{\rm jet}$, $\mathcal{U}_{\rm host}$, $\mathcal{U}_{\rm clu}$, $\mathcal{U}_{\rm ext}$ and $\mathcal{U}_{\rm MW}$ of the photon-ALP beam propagating in the regions described above, we can evaluate the total transfer matrix of the system $\mathcal{U}$ which reads

$$\mathcal{U} = \mathcal{U}_{\rm MW}\mathcal{U}_{\rm ext}\mathcal{U}_{\rm clu}\mathcal{U}_{\rm host}\mathcal{U}_{\rm jet}. \tag{17}$$

By combining Eqs. (6) and (17), we obtain the photon survival probability of photons produced in the jet and oscillating into ALPs up to us

$$P_{\gamma\to\gamma} = \sum_{i=x,z} \mathrm{Tr}[\rho_i \mathcal{U} \rho_{\rm in} \mathcal{U}^\dagger], \tag{18}$$

where ρ_x and ρ_z are given by Eq. (7) and $\rho_{\rm in}$ is the beam initial polarization density matrix. Furthermore, $\rho_{\rm in}$ is derived from the expression of the initial photon degree of linear polarization $\Pi_{L,0}$ defined in the next subsections for the different sources. The final photon degree of linear polarization Π_L and the polarization angle χ are evaluated by means of Eqs. (11) and (12), respectively by recalling Eq. (5) with $\rho_0 \equiv \rho_{\rm in}$ (for more details see [26,48,49]).

Finally, one point should be kept in mind. Due to the fact that the extragalactic magnetic field domains are randomly distributed and since we also consider the turbulent component of the Milky Way magnetic field, the photon-ALP beam propagation becomes a *stochastic process* and several realizations of it must be evaluated in order to infer its statistical properties and the robustness of our results. Yet, the photon-ALP beam can physically experience only one realization at once.

IV. RESULTS

Before proceeding to present our results, we must deal with a technological problem, which may limit the effectiveness of our findings. Since real polarimeters in the considered bands are satellite borne, they possess a small spatial resolution, and so we cannot distinguish photons coming from different regions inside the transverse section of the blazar jet. As a consequence, all photons are collected together and the polarization features may be washed out by the averaging procedure on all photons from the jet [109].

We must keep in mind that we observe emitted photons equally distributed on the jet section only in the case of a perfect alignment between the line of sight and the jet axis i.e. when $\theta_{\rm com} = \theta_{\rm fix} = 0$, where $\theta_{\rm com}$ represents the angle between the jet axis and the photon-ALP beam propagation direction *in the jet comoving frame*, while $\theta_{\rm fix}$ is the same angle but as observed *in the fixed external frame*. This is an extreme situation. The other extreme option is represented by photons emitted perpendicularly to the jet axis *in the jet comoving frame* so that $\theta_{\rm com} = \pi/2$, with the resulting photons propagating along the external border of the jet with $\theta_{\rm fix} = 1/\gamma$ (for the geometry of both the two extreme cases see Fig. 19 in [48]). The probability of being in one of the previous situations is obviously vanishingly small.

Realistically, we are in an intermediate situation, wherein photons propagate up to the Earth not along the jet axis and not close to the external conical border of the jet. Merely for statistical reasons, the region of close alignment is much less probable. Therefore, photons coming from a specific small zone in the jet transverse section are much more probable than the others (see [48] for a complete description of the problem and for the adopted strategy of evaluation). We take this fact into account by weighting

the photons by means of a Gaussian distribution centered on the region of the jet section, where the maximal amount of photons reaching us are produced (see [48] for details).

Since the intermediate case is the only interesting one for real applications and represents what occurs in practice, we shall be concerned with such a situation only. In order to be conservative, we use the same magnetic field profile as reported in Eq. (15) and a propagation distance in the jet of 1 pc. As benchmark value we consider $\theta_{\rm com} = 3\pi/10$ resulting in $\theta_{\rm fix} \simeq 1/(2\gamma)$. Apart from the unrealistic case $\theta_{\rm com} = \theta_{\rm fix} = 0$, a variation of $\theta_{\rm com}$ does not produce strong modifications to the final Π_L, as shown in Fig. 20 of [48].

We are now in a position to present our results about the final photon survival probability $P_{\gamma\to\gamma}$, the corresponding photon degree of linear polarization Π_L and polarization angle χ when photons are emitted at the jet base of the following BL Lacs: OJ 287, BL Lacertae, Markarian 501 and 1ES 0229 + 200, and oscillate into ALPs in all the magnetized regions crossed by the photon-ALP beam (blazar jet, host galaxy, extragalactic space and Milky Way). Since the real nature of $\mathbf{B}_{\rm ext}$ and of other crossed turbulent magnetic fields is unknown, we evaluate several realizations of the photon-ALP beam propagation process by varying the magnetic field parameters, and we compute the probability density function f_Π associated with the final Π_L for the different realizations.

We take ALP parameters within current bounds: $g_{a\gamma\gamma} = 0.5 \times 10^{-11}$ GeV^{-1} and the two ALP mass values: (i) $m_a \lesssim 10^{-14}$ eV, (ii) $m_a = 10^{-10}$ eV. We consider photons emitted at redshift z with energy E and with observed energy $E_0 = E/(1+z)$ in the two ranges: (i) UV-x-ray band (4×10^{-2} keV–10^2 keV), and (ii) HE band (10^{-1} MeV–5×10^2 MeV). In Fig. 1 we report the *initial* photon degree of linear polarization $\Pi_{L,0}$ for the BL Lacs

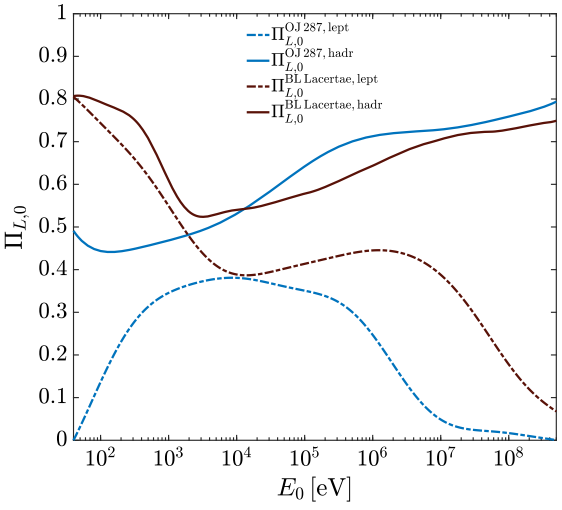

FIG. 1. Initial degree of linear polarization $\Pi_{L,0}$ for the blazars OJ 287 and BL Lacertae in the case of both leptonic and hadronic emission mechanisms, as derived in [110].

OJ 287 and BL Lacertae both in the leptonic and the hadronic scenarios, as derived in [110]. Instead, we take $\Pi_{L,0} = 0.3$ in the UV-x-ray band for Markarian 501 in the leptonic model and the same value also for 1ES 0229 + 200 in both the leptonic and the hadronic cases (more about this, below).

Note that values of $\Pi_{L,0}$ larger than those considered here are at least unlikely because they should be produced in the x-ray band by the electron-synchrotron emission mechanism and in the HE range by the proton-synchrotron emission mechanism with an unphysically extremely high ordered $\mathbf{B}^{\rm jet}$. Realistically, some degree of turbulence is expected for $\mathbf{B}^{\rm jet}$ preventing extremely high values of $\Pi_{L,0}$, as shown by recent IXPE results [111–113].

In the following figures concerning the final Π_L and χ for all considered BL Lacs, we show also binned data of our results, in order to figure out how a possible detection of ALP-induced features may appear. The binning procedure takes the energy resolution of current polarimeters into account, which is expected to be worse with respect to spectrum-measuring observatories in the x-ray band [114] by a factor 4–5. In the HE range the energy resolution of spectral and polarization measurements is expected to be similar, as they derive from the same data [56–58]. Correspondingly, we take 15–20 bins per decade in the x-ray band and, conservatively, 8–10 bins per decade in the HE range (see also [115] concerning the binning procedure).

A final remark is in order: in all the following figures concerning χ, a phase flip of π is simply due to the periodicity of the function χ in Eq. (12). Instead, a phase flip of $\sim\pi/2$ for χ in correspondence with a vanishing Π_L is caused by the behavior of the Stokes parameters Q and U entering the definition of Π_L and χ in Eqs. (11) and (12), respectively. In particular, the condition $\Pi_L \to 0$ arises from $Q \to 0$ and $U \to 0$. In the case of $Q \to 0$ and $U \to 0$ but with a variation in the sign of U/Q, the analytic expression of Eq. (12) produces a phase flip of $\sim\pi/2$ in χ. Note that all the Stokes parameters always vary continuously.

A. OJ 287

OJ 287 is a low-frequency peaked blazar (LBL) observed at redshift $z = 0.3056$. It is considered as a good observational target for polarimetric studies both in the x-ray and HE range because of the high flux in both these energy bands [110]. We consider both a leptonic and hadronic emission model: correspondingly, we assume the typical LBL parameter values $B_0^{\rm jet} = 1$ G, $y_{\rm em} = 3 \times 10^{16}$ cm and $\gamma = 10$ for the leptonic case and $B_0^{\rm jet} = 20$ G, $y_{\rm em} = 10^{17}$ cm and $\gamma = 15$ concerning the hadronic one [116]. The assumed initial degree of linear polarization $\Pi_{L,0}$ for both leptonic and hadronic scenarios is reported in Fig. 1. Finally, we take $g_{a\gamma\gamma} = 0.5 \times 10^{-11}$ GeV^{-1}.

We start by considering the case of an ALP mass $m_a \lesssim 10^{-14}$ eV. Our results concerning the UV-x-ray band

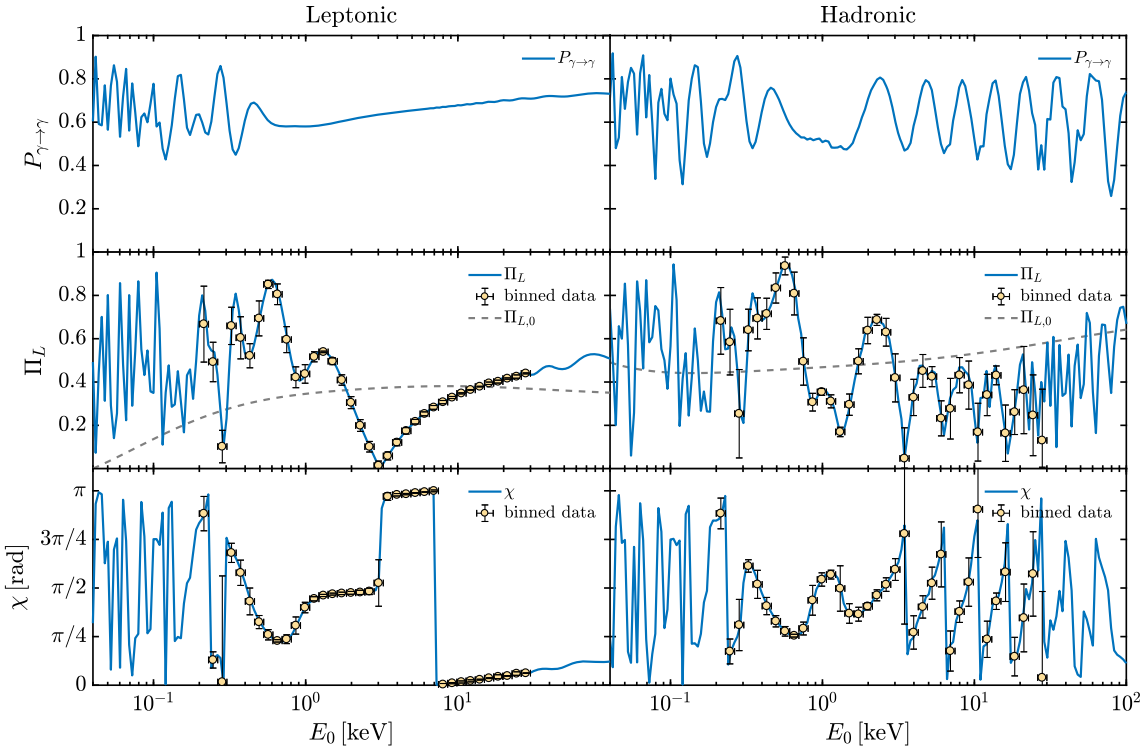

FIG. 2. OJ 287: photon survival probability $P_{\gamma\to\gamma}$ (upper panels), corresponding final degree of linear polarization Π_L (central panels) and final polarization angle χ (lower panels) in the energy range $(4\times10^{-2}$–$10^2)$ keV. We take $g_{a\gamma\gamma}=0.5\times10^{-11}$ GeV^{-1}, $m_a\lesssim10^{-14}$ eV. We consider a leptonic and hadronic emission mechanism in the left and right column, respectively. Correspondingly, the initial degree of linear polarization $\Pi_{L,0}$ is also shown (see also Fig. 1).

$(4\times10^{-2}$ keV–10^2 keV) are shown in Figs. 2 and 3. In particular, we report $P_{\gamma\to\gamma}$ in the top panel of Fig. 2 and the corresponding final Π_L and χ in the central and lower panel of Fig. 2, respectively. As the photon-ALP beam propagates in the weak mixing regime because of the significant contribution of the plasma term (see also [62]), Fig. 2 shows an energy dependence of $P_{\gamma\to\gamma}$ and of the corresponding final Π_L which is strongly modified with respect to the initial $\Pi_{L,0}$

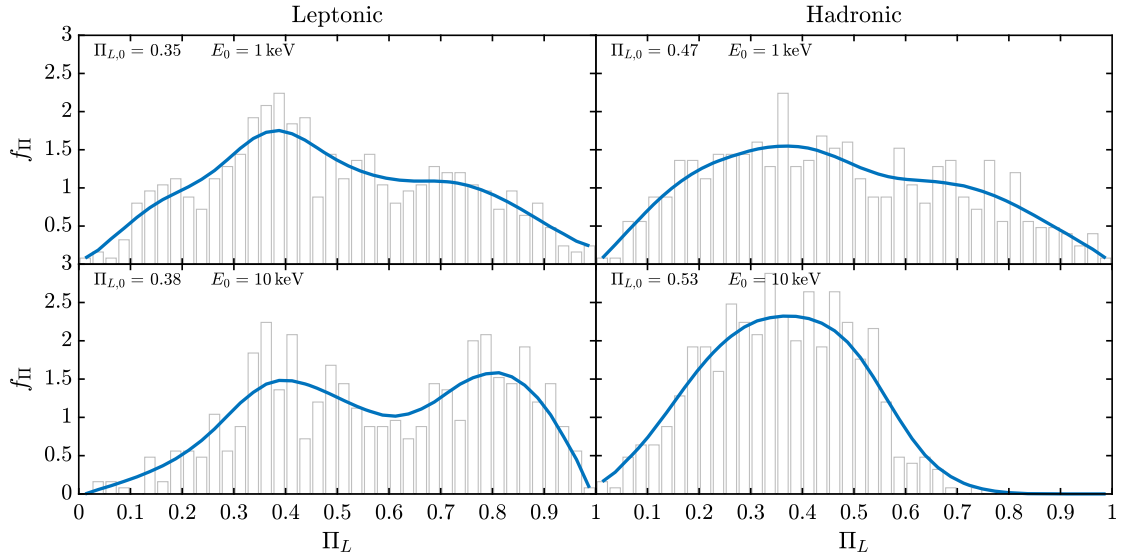

FIG. 3. OJ 287: probability density function f_Π obtained by interpolating the plotted histogram for the final degree of linear polarization Π_L at 1 keV (upper panels) and 10 keV (lower panels) by considering the system in Fig. 2. We address a leptonic and hadronic emission mechanism in the left and right column, respectively. Correspondingly, the initial degree of linear polarization $\Pi_{L,0}$ is provided in Fig. 1.

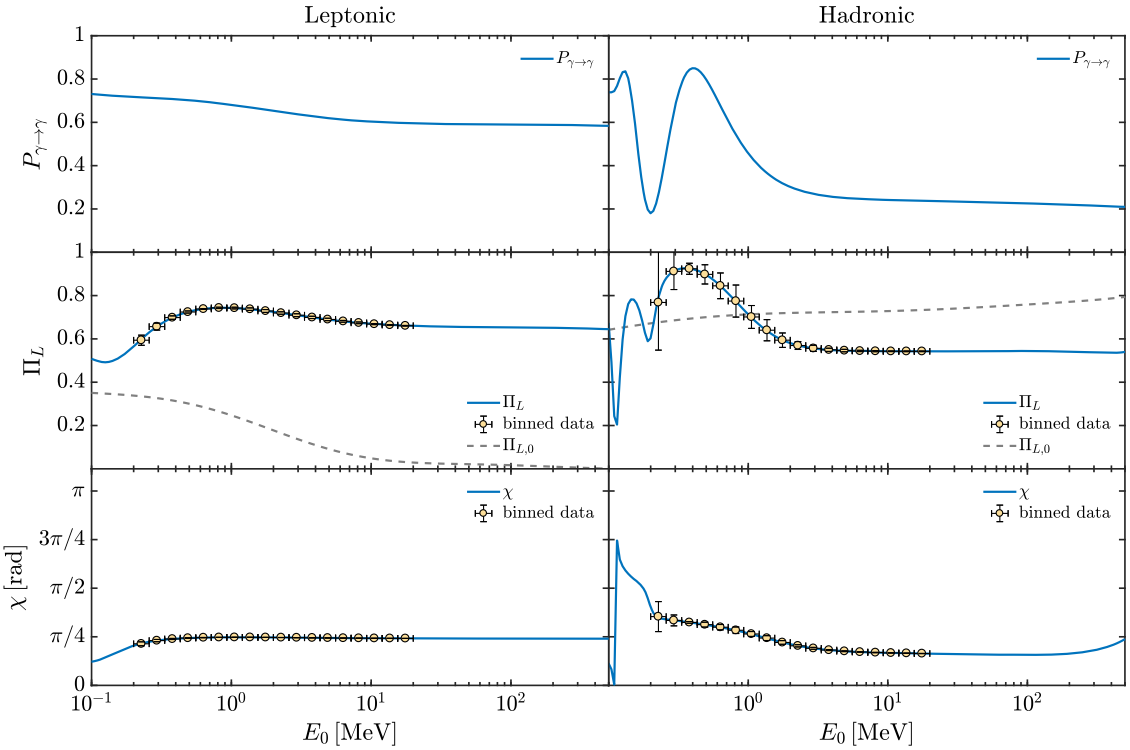

FIG. 4. OJ 287: same as Fig. 2 but in the energy range $(10^{-1}$–$5\times10^{2})$ MeV. We take $g_{a\gamma\gamma}=0.5\times10^{-11}$ GeV^{-1}, $m_a\lesssim10^{-14}$ eV.

both in the leptonic and in the hadronic cases. As noted in [48], the weak mixing regime is not limited to a small energy range but extends for several energy decades because of the high variation of $B^{\rm jet}$ and $n_e^{\rm jet}$ [see Eqs. (15) and (16), respectively]. This remark applies to all the following cases wherein the system, for different parameters values, lies in the weak mixing regime. The binned data in Fig. 2 indicate that the high variability of Π_L in both the leptonic and the hadronic cases can be detected by IXPE [50], eXTP [51], XL-Calibur [52], NGXP [53] and XPP [54] for $E_0\gtrsim0.5$ keV. As confirmed by the behavior of χ in Fig. 2, we see that the hadronic case shows a higher energy variability as compared to the leptonic case because of the larger size of the jet region and of the corresponding value of $B_0^{\rm jet}$.

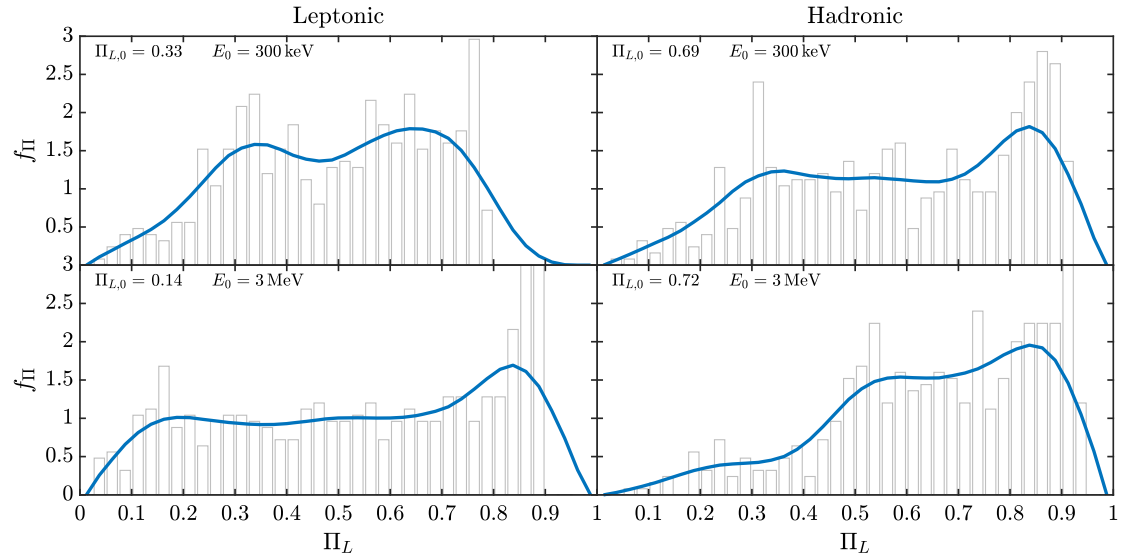

FIG. 5. OJ 287: same as Fig. 3 but for the energies 300 keV (upper panels) and 3 MeV (lower panels) by considering the system in Fig. 4.

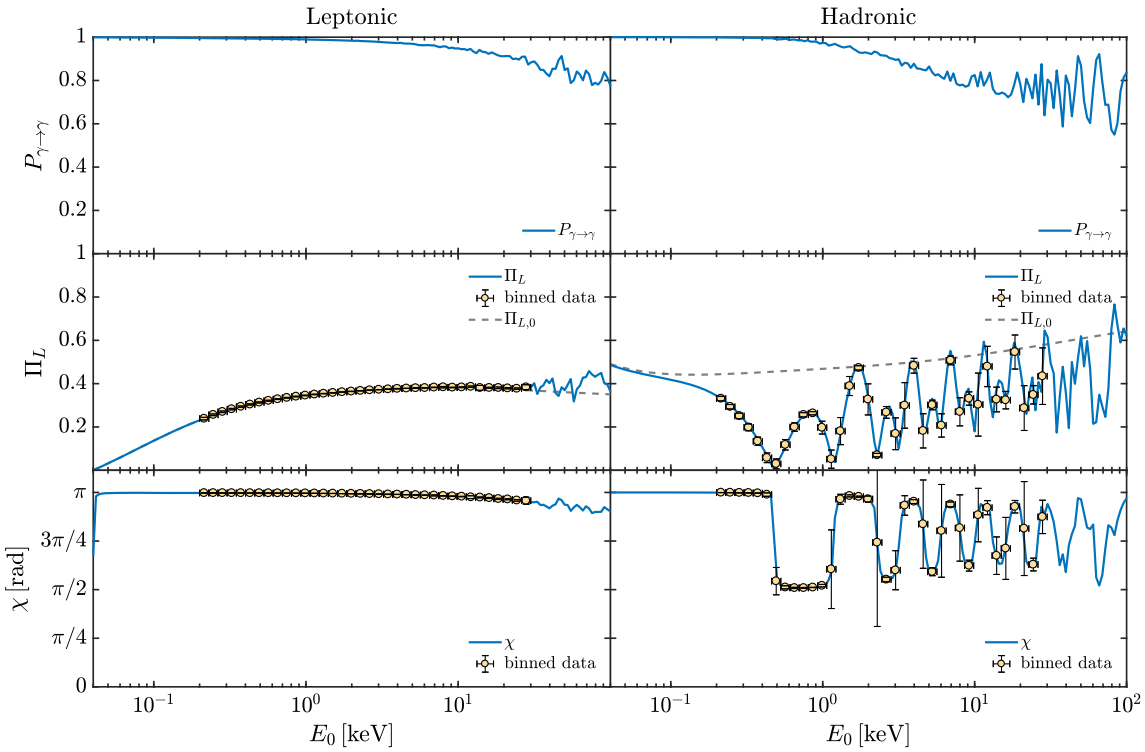

FIG. 6. OJ 287: same as Fig. 2. We take $g_{a\gamma\gamma} = 0.5 \times 10^{-11}$ GeV^{-1}, $m_a = 10^{-10}$ eV.

Because the final $P_{\gamma\to\gamma}$ and the corresponding final Π_L and χ depend on the particular choice of the orientation and coherence length of $\mathbf{B}_{\rm ext}$ (and of the other turbulent magnetic fields) but only the statistical properties of these quantities are known, our results in Fig. 2 are obtained for a particular realization of the photon-ALP beam propagation process. But in order to infer its statistical properties and the robustness of our results several realizations must be considered. Consequently, we report the probability density function f_Π for the final Π_L of all realizations in Fig. 3, where we consider the two benchmark energies $E_0 =$ 1 keV and $E_0 = 10$ keV. In all cases, we observe a broadening of the initial $\Pi_{L,0}$. For the hadronic case we generally find a decrease of the initial $\Pi_{L,0}$, while in the leptonic case and for $E_0 = 10$ keV the most probable result is $\Pi_L \gtrsim 0.8$, which is much higher than that predicted by

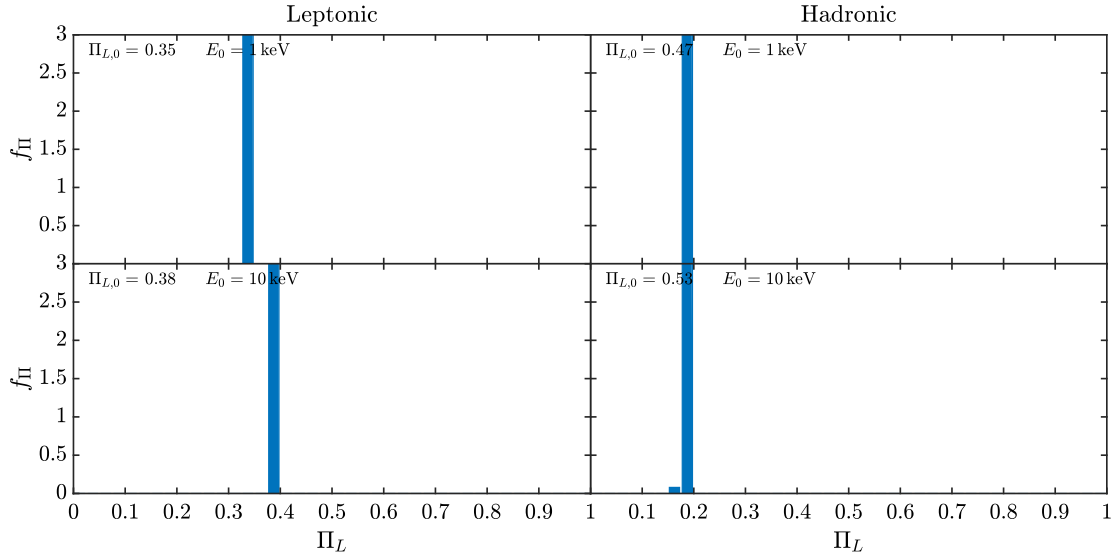

FIG. 7. OJ 287: same as Fig. 3 by considering the system in Fig. 6.

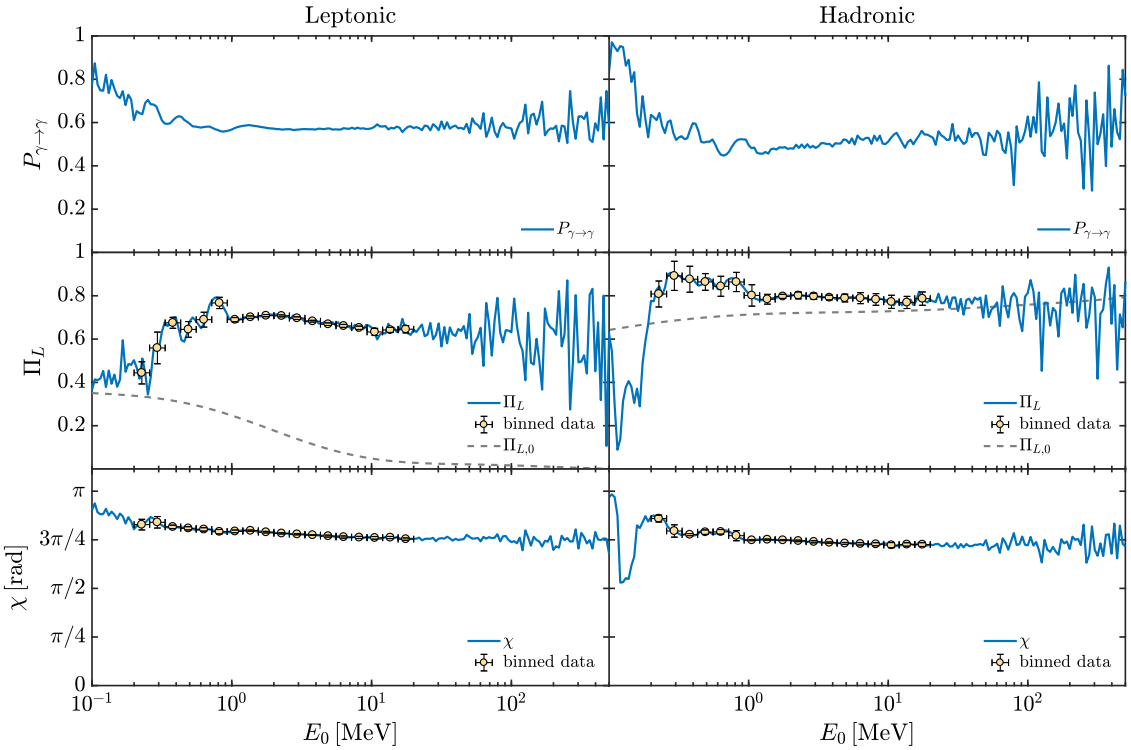

FIG. 8. OJ 287: same as Fig. 4. We take $g_{a\gamma\gamma} = 0.5 \times 10^{-11}$ GeV^{-1}, $m_a = 10^{-10}$ eV.

conventional physics in both emission mechanisms. Thus, the detectability of the last feature appears robust.

In the HE band we focus our attention on the range $(10^{-1}$–$5 \times 10^2)$ MeV—and we follow the same strategy described above. Therefore, in both the leptonic and the hadronic cases we report $P_{\gamma\to\gamma}$, the related final Π_L and χ for a particular realization of the photon-ALP beam propagation process in Fig. 4, while the associated statistical properties obtained by considering all different realizations are shown in Fig. 5, where we plot the corresponding f_Π. Since in both the leptonic and the hadronic scenarios the photon-ALP mixing term dominates over all the other effects (see also [62]) in almost the whole HE band, we see in Fig. 4 that the photon-ALP beam propagates in the strong mixing regime, so that the resulting binned data are almost energy independent, presenting less

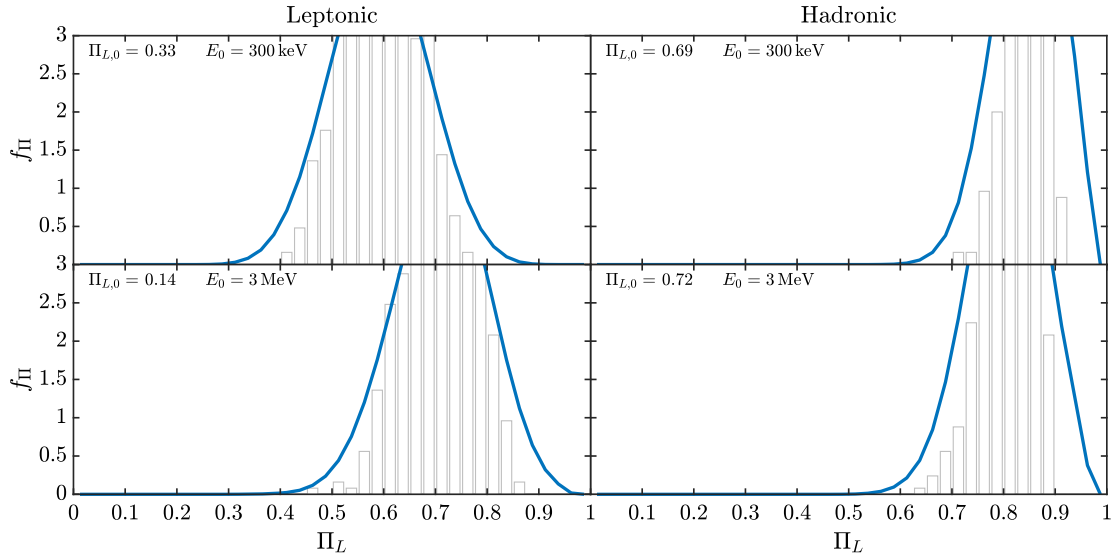

FIG. 9. OJ 287: same as Fig. 5 by considering the system in Fig. 8.

uncertainties than in the UV-x-ray band. As a result, OJ 287 appears as a good target for observatories such as COSI [55], e-ASTROGAM [56,57] and AMEGO [58]. In Fig. 5 the behavior of f_Π shows that in both the leptonic and the hadronic cases and for both the considered energies $E_0 =$ 300 keV and $E_0 = 3$ MeV the final Π_L is broadened. The case $E_0 = 3$ MeV appears as the most promising one both in the leptonic and the hadronic scenarios, since the most probable value for the final Π_L is $\Pi_L \gtrsim 0.8$, which is larger than that predicted by conventional physics in both emission mechanisms.

We now turn to the case of an ALP mass $m_a = 10^{-10}$ eV by proceeding as above. In the UV-x-ray band the ALP mass term is so strong that in the leptonic scenario dominates in all regions crossed by the photon-ALP beam. As a consequence, the final Π_L is not modified since the photon-ALP conversion is totally inefficient, as shown by the left panels of Fig. 6 and by the behavior of f_Π in the left panels of Fig. 7. Instead, in the hadronic case, the photon-ALP conversion is sizable but only in the jet for the higher central value of $B_0^{\rm jet} = 20$ G with a resulting dimming of the initial $\Pi_{L,0}$ (see the behavior of Π_L in the right panels of Fig. 6 and that of f_Π in the right panels of Fig. 7). In the present situation we have no substantial broadening in the final values of Π_L for both $E_0 = 1$ keV and $E_0 = 10$ keV, as shown in the right panels of Fig. 7, since the photon-ALP conversion in the extragalactic space—which is the maximal responsible for the broadening in the other cases—is totally negligible.

In the HE band, the photon-ALP beam propagates in the weak mixing regime both in the leptonic and hadronic scenario, so that $P_{\gamma\to\gamma}$ and the corresponding final Π_L and χ turn out to be energy dependent as shown in Fig. 8. As a general trend, we observe an increase of the initial $\Pi_{L,0}$. We infer from the binned data that observatories like COSI [55], e-ASTROGAM [56,57] and AMEGO [58] can detect the above features for $E_0 \gtrsim (0.2\text{–}2)$ MeV. The behavior of f_Π in Fig. 9 confirms that the most probable final values of Π_L increase with respect to the initial $\Pi_{L,0}$ with a moderate broadening for both the two considered benchmark energies $E_0 = 300$ keV and $E_0 = 3$ MeV.

B. BL Lacertae

BL Lacertae is the prototype of the AGN class called BL Lacertae object (BL Lac). In particular, it is an intermediate-frequency peaked blazar (IBL) and has been observed at redshift $z = 0.069$. Due to its relative proximity to the Earth and to its high flux in both the UV-x-ray and HE ranges, BL Lacertae is regarded as a good observational target for polarimetric studies in both bands [110]. Similarly to OJ 287, we take both a leptonic and a hadronic emission model into account. We assume the following typical IBL parameter values: $B_0^{\rm jet} = 1$ G, $y_{\rm em} = 3 \times 10^{16}$ cm and $\gamma = 10$ for the leptonic case, and $B_0^{\rm jet} = 20$ G, $y_{\rm em} = 10^{17}$ cm and $\gamma = 15$ concerning the hadronic one [116]. In either case we choose as before $g_{a\gamma\gamma} = 0.5 \times 10^{-11}$ GeV^{-1}. For both the leptonic and the hadronic scenarios, the initial degree of linear polarization $\Pi_{L,0}$ is shown in Fig. 1.

Since OJ 287 and BL Lacertae possess similar features, they show comparable ALP-induced effects on the final photon polarization. This is the reason why we refer the reader to the previous subsection about OJ 287 for a complete discussion about the results concerning BL Lacertae, while here we merely stress the few differences between the two sources.

For an ALP mass $m_a \lesssim 10^{-14}$ eV, we exhibit our results concerning the UV-x-ray band in Figs. 10 and 11, while our findings for the HE range are reported in Figs. 12 and 13. In these cases, for BL Lacertae we do not observe substantial modifications with respect to what we found for OJ 287, apart from a less evident pseudo-oscillatory behavior of $P_{\gamma\to\gamma}$, and of the corresponding final Π_L and χ especially in the UV-x-ray band, as reported in Fig. 10 (if compared to Fig. 2) and a lower broadening of the final values of Π_L, as shown in Fig. 11 (see Fig. 3 for comparison). The reason for this behavior is that BL Lacertae is closer to the Earth than OJ 287. Thus, the photon-ALP conversion in the extragalactic space—which is the main reason for these effects—is less effective. In the HE range, we do not find substantial modifications with respect to OJ 287 if we compare Π_L in Fig. 12 with Fig. 4 and f_Π in Fig. 13 with Fig. 5.

In the case of an ALP mass $m_a = 10^{-10}$ eV, our results for the UV-x-ray band are reported in Figs. 14 and 15, while our findings for the HE range are shown in Figs. 16 and 17. In these cases the behavior of BL Lacertae is totally similar to that of OJ 287, apart from the left panels of Figs. 14 and 15 concerning Π_L and f_Π, respectively, if compared to the left panels of Figs. 6 and 7. The reason for that lies in the fact that in the leptonic scenario and in the case $m_a = 10^{-10}$ eV, the photon-ALP conversion is negligible in the UV-x-ray band, so that the difference between BL Lacertae and OJ 287 is only due to their different initial values of $\Pi_{L,0}$ (see Fig. 1).

Overall, also BL Lacertae represents a good observational target for ALP studies with IXPE [50], eXTP [51], XL-Calibur [52], NGXP [53] and XPP [54] in the x-ray band and with COSI [55], e-ASTROGAM [56,57] and AMEGO [58] in the HE range especially in the cases discussed for OJ 287.

C. Markarian 501

Markarian 501 is a high-frequency peaked blazar (HBL) detected at redshift $z = 0.034$. As a HBL, Markarian 501 possesses the synchrotron peak at x-ray energies, which makes it an ideal target for polarization studies in such energy band. However, the valley between the synchrotron and the VHE peak lies in the HE range at about a few MeV, so that Markarian 501 is not an ideal target for polarization analyses in the HE band. Concerning the emission mechanism, we consider only a leptonic scenario with typical

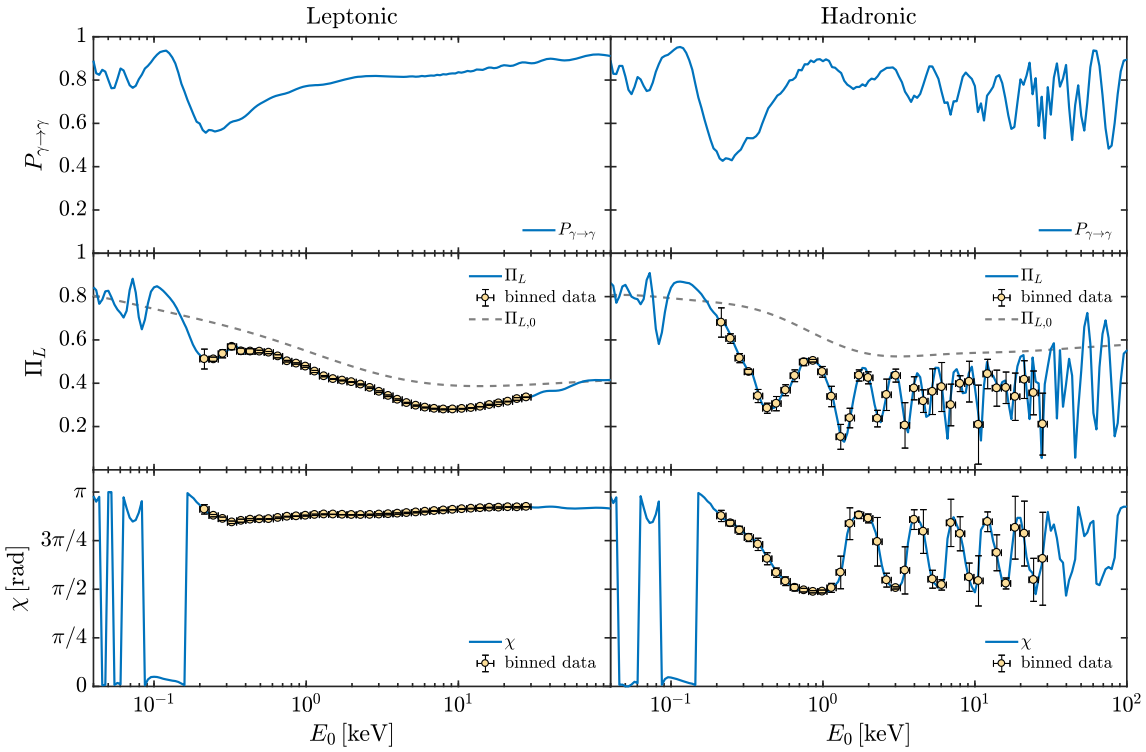

FIG. 10. BL Lacertae: photon survival probability $P_{\gamma\to\gamma}$ (upper panels), corresponding final degree of linear polarization Π_L (central panels) and final polarization angle χ (lower panels) in the energy range $(4\times10^{-2}$–$10^2)$ keV. We take $g_{a\gamma\gamma}=0.5\times10^{-11}$ GeV^{-1}, $m_a\lesssim10^{-14}$ eV. We consider a leptonic and hadronic emission mechanism in the left and right column, respectively. Correspondingly, the initial degree of linear polarization $\Pi_{L,0}$ is also shown (see also Fig. 1).

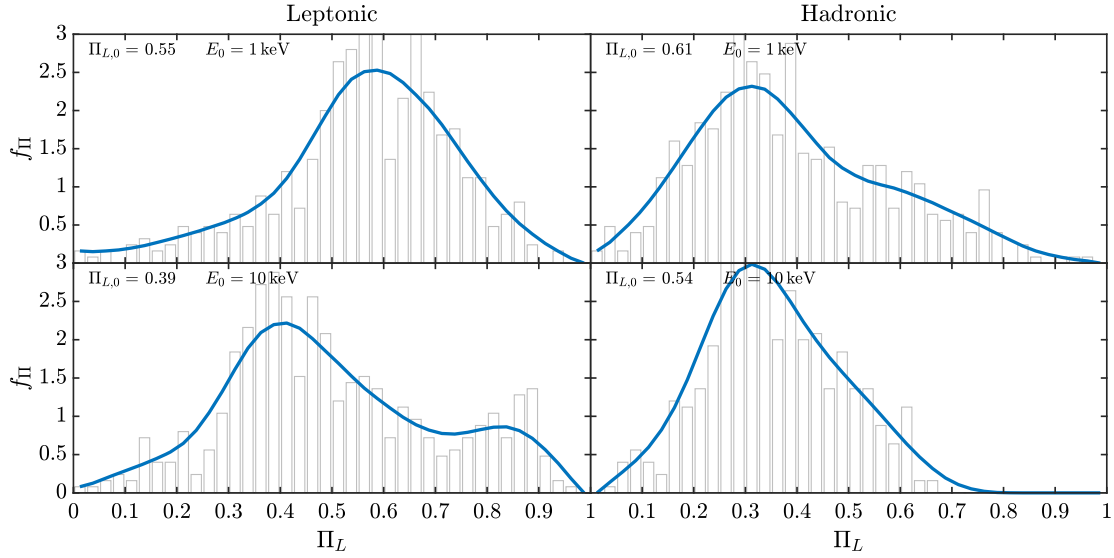

FIG. 11. BL Lacertae: probability density function f_Π obtained by interpolating the plotted histogram for the final degree of linear polarization Π_L at 1 keV (upper panels) and 10 keV (lower panels) by considering the system in Fig. 10. We address a leptonic and hadronic emission mechanism in the left and right column, respectively. Correspondingly, the initial degree of linear polarization $\Pi_{L,0}$ is provided in Fig. 1.

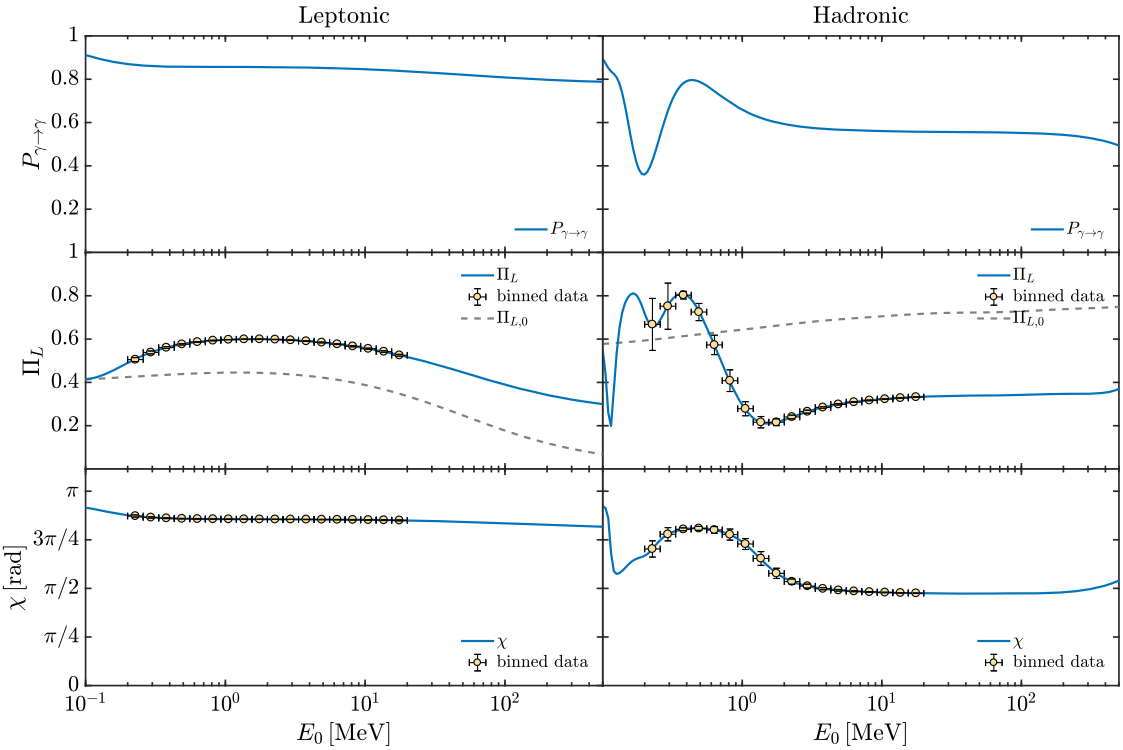

FIG. 12. BL Lacertae: same as Fig. 10 but in the energy range $(10^{-1}$–$5\times10^{2})$ MeV. We take $g_{a\gamma\gamma}=0.5\times10^{-11}$ GeV^{-1}, $m_a\lesssim10^{-14}$ eV.

HBL parameter values: $B_0^{\rm jet}=0.5$ G, $y_{\rm em}=3\times10^{16}$ cm and $\gamma=15$ [117], since the hadronic emission mechanism cannot be applied owing to the high variability of the source. As the central $B_0^{\rm jet}$ is not so high, we cannot observe ALP-induced effects on photon polarization for an ALP mass $m_a=10^{-10}$ eV in the UV-x-ray band, as already pointed out in the previous two subsections. This is the reason why we concentrate in the following only on the case $m_a\lesssim10^{-14}$ eV, taking again $g_{a\gamma\gamma}=0.5\times10^{-11}$ GeV^{-1}. Since ALPs induce a modification of the final photon polarization, we choose an initial degree of linear polarization $\Pi_{L,0}=0.3$ as an upper limit to $\Pi_{L,0}$ [118].

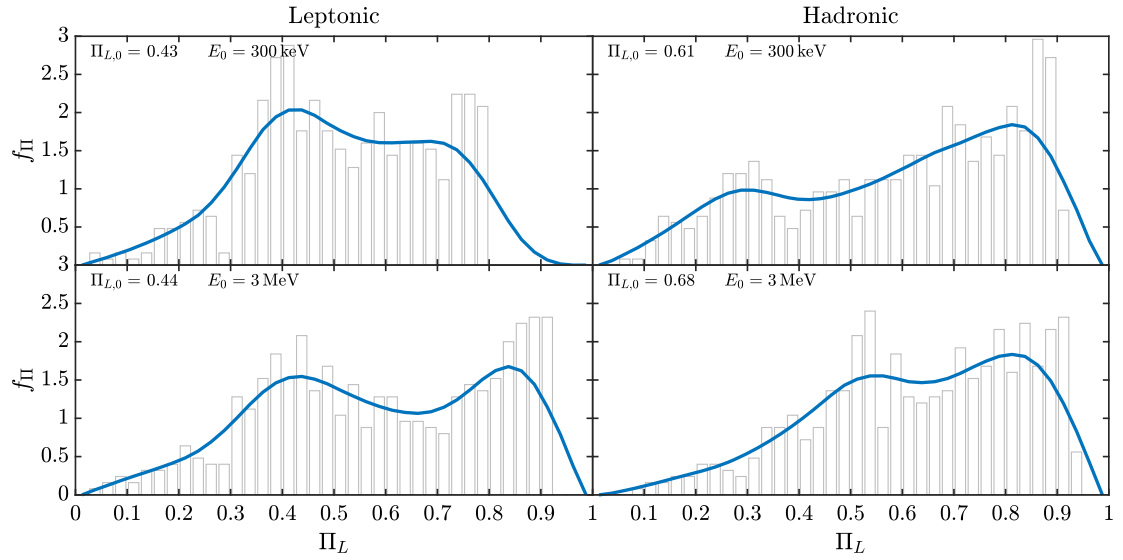

FIG. 13. BL Lacertae: same as Fig. 11 but for the energies 300 keV (upper panels) and 3 MeV (lower panels) by considering the system in Fig. 12.

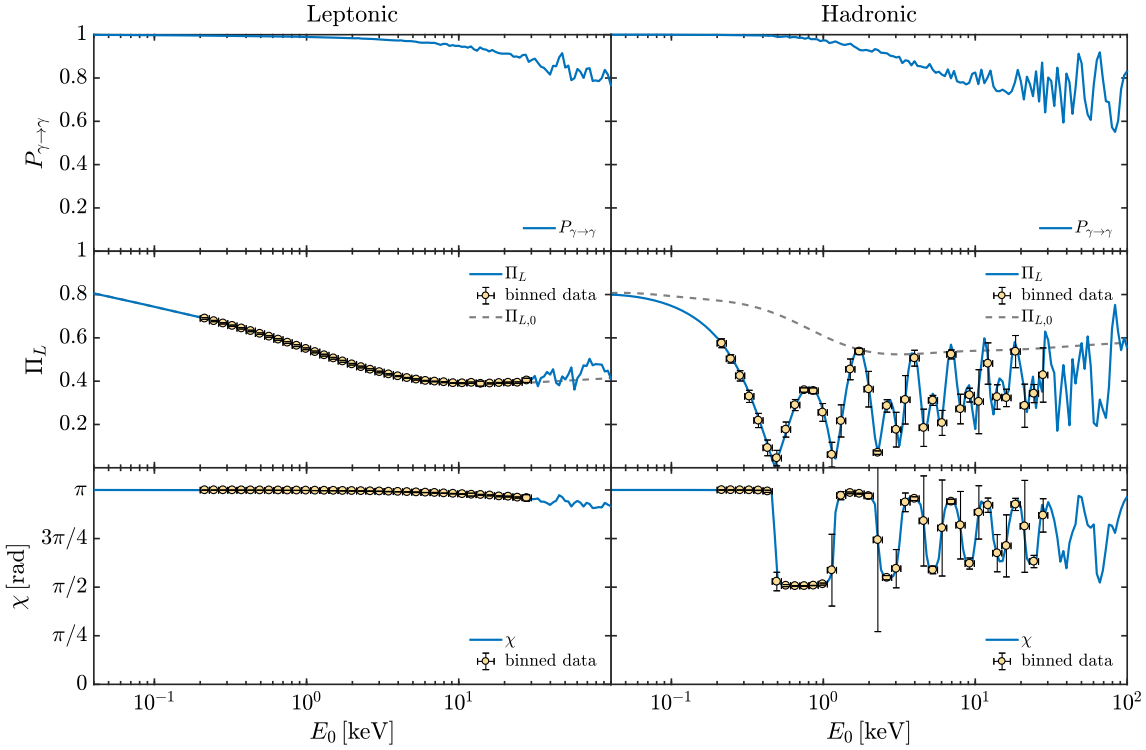

FIG. 14. BL Lacertae: same as Fig. 10. We take $g_{a\gamma\gamma} = 0.5 \times 10^{-11}$ GeV^{-1}, $m_a = 10^{-10}$ eV.

In Fig. 18, we report $P_{\gamma\to\gamma}$ and the corresponding final Π_L and χ. The photon-ALP system is in the weak mixing regime in the most of the considered energy band (4×10^{-2} keV–10^2 keV) so that $P_{\gamma\to\gamma}$, Π_L and χ turn out to be energy dependent. However, the final Π_L appears not to be strongly modified by the photon-ALP oscillations. In fact, the binned data in Fig. 18 present a weak variability with small error bars. For both the benchmark energies $E_0 = 1$ keV and $E_0 = 10$ keV, Fig. 19 confirms our previous statement: the behavior of f_Π shows that the most probable value for the final Π_L is still close to the initial one $\Pi_L \simeq \Pi_{L,0} = 0.3$ with a moderate broadening in the range 0.1–0.5. Note that Fig. 19 is compatible with the recent IXPE results [112].

The reason for the different behavior of Markarian 501 with respect to the previously considered BL Lacs is

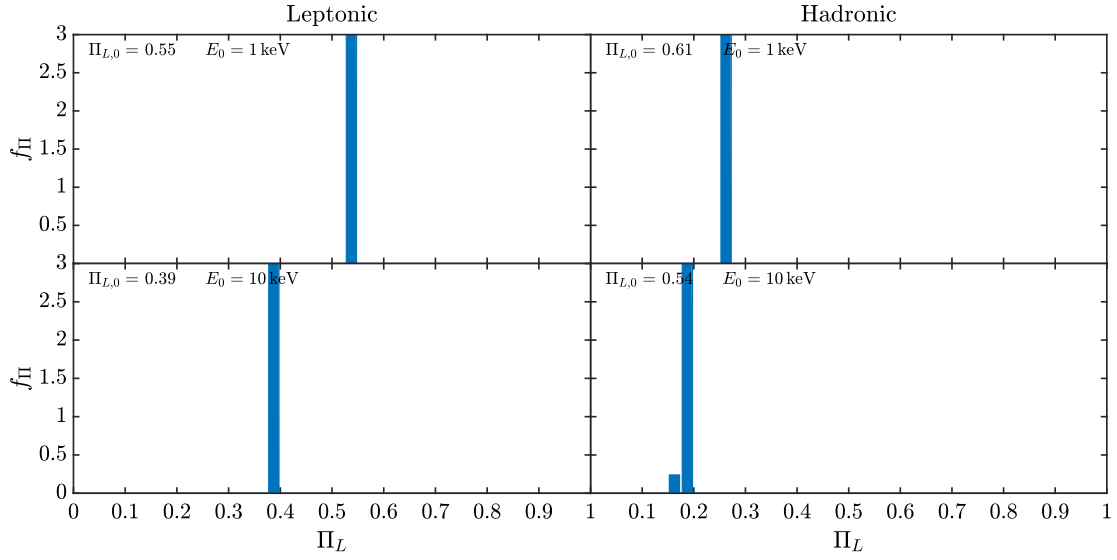

FIG. 15. BL Lacertae: same as Fig. 11 by considering the system in Fig. 14.

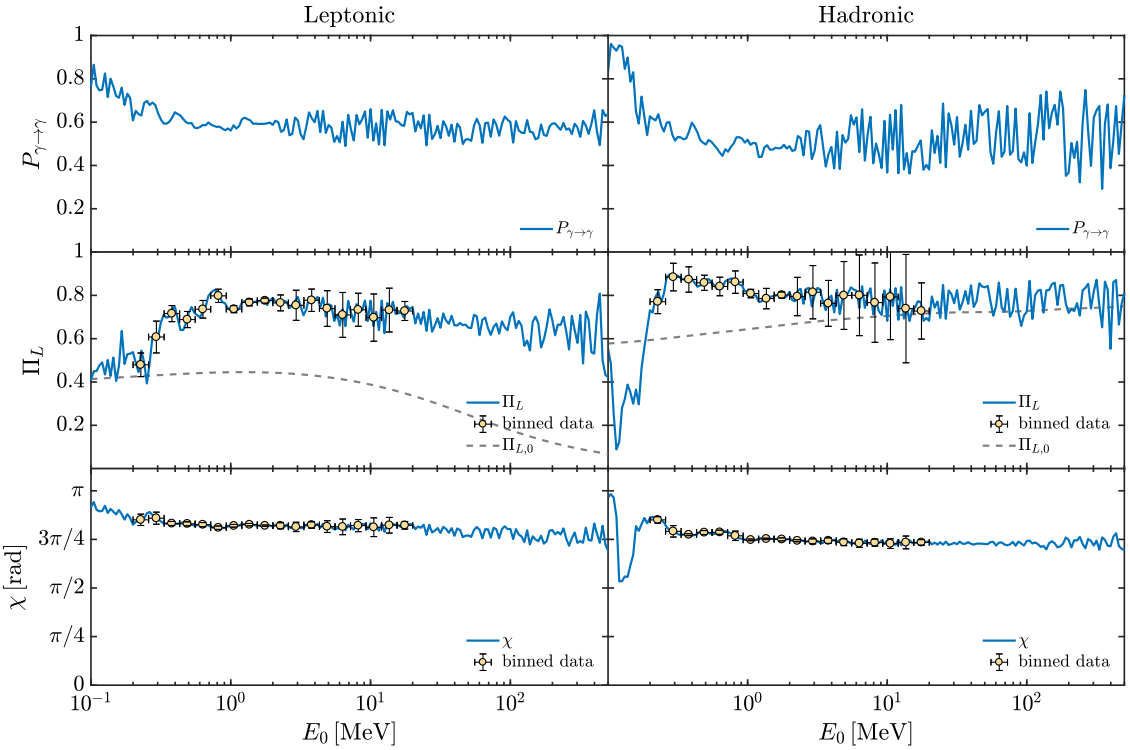

FIG. 16. BL Lacertae: same as Fig. 12. We take $g_{a\gamma\gamma} = 0.5 \times 10^{-11}$ GeV^{-1}, $m_a = 10^{-10}$ eV.

twofold. First, the lower value of its central $B_0^{\rm jet}$—with respect to the previous cases—cannot substantially modify the photon polarization. Second, the relative proximity of Markarian 501 to the Earth implies a smaller broadening of the final photon polarization. For these reasons Markarian 501 does not appear as the best observational target for studies of ALP-induced effects on photon polarization in the x-ray band with observatories such as IXPE [50], eXTP [51], XL-Calibur [52], NGXP [53] and XPP [54].

D. 1ES 0229 + 200

1ES 0229 + 200 is the prototype of the so-called extreme HBLs (EHBLs, [119,120]) and has been observed at redshift $z = 0.1396$. Similarly to Markarian 501 it shows the synchrotron peak at x-ray energies, and it exhibits the valley between the synchrotron and the VHE peak in the HE range at about a few MeV. Therefore, 1ES 0229 + 200 represents an excellent observational target for polarization studies in

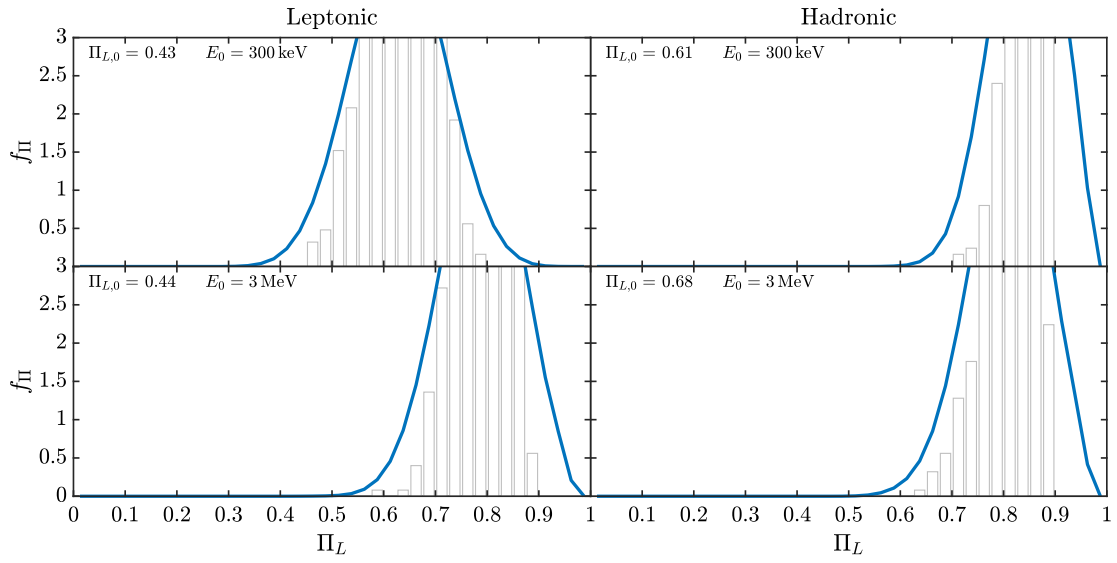

FIG. 17. BL Lacertae: same as Fig. 13 by considering the system in Fig. 16.

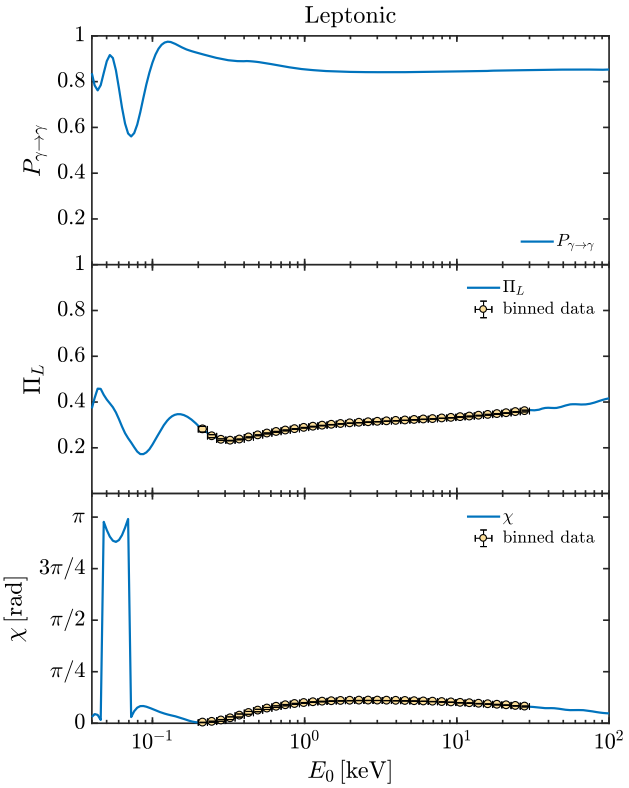

FIG. 18. Markarian 501: photon survival probability $P_{\gamma\to\gamma}$ (upper panel), corresponding final degree of linear polarization Π_L (central panel) and final polarization angle χ (lower panel) in the energy range $(4\times10^{-2}$–$10^2)$ keV. We take $g_{a\gamma\gamma}=0.5\times10^{-11}$ GeV^{-1}, $m_a\lesssim10^{-14}$ eV. The initial degree of linear polarization is $\Pi_{L,0}=0.3$.

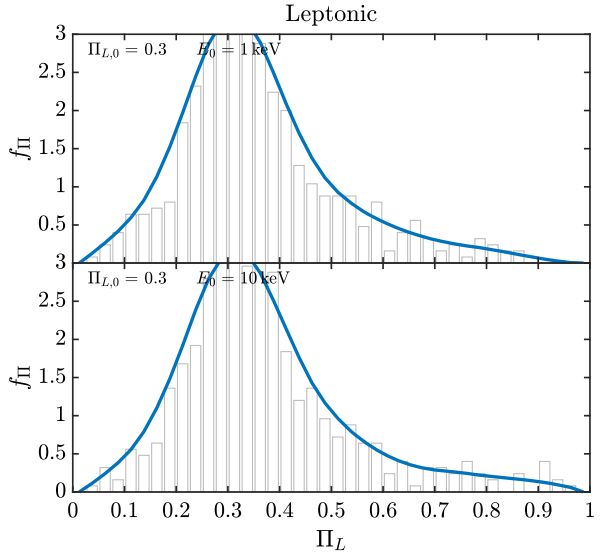

FIG. 19. Markarian 501: probability density function f_Π obtained by interpolating the plotted histogram for the final degree of linear polarization Π_L at 1 keV (upper panel) and 10 keV (lower panel) by considering the system in Fig. 18. The initial degree of linear polarization is $\Pi_{L,0}=0.3$.

the x-ray band but not in the HE range. We contemplate both the leptonic and the hadronic emission mechanisms. Correspondingly, we assume the typical EHBL parameter values $B_0^{\rm jet}=2$ mG, $y_{\rm em}=3\times10^{16}$ cm and $\gamma=50$ for the leptonic case and $B_0^{\rm jet}=0.5$ G, $y_{\rm em}=3\times10^{16}$ cm and $\gamma=15$ regarding the hadronic one [119,120]. Once again we assume $g_{a\gamma\gamma}=0.5\times10^{-11}$ GeV^{-1}. In the following, we investigate only the case $m_a\lesssim10^{-14}$ eV for the same reasons explained for Markarian 501, namely the central $B_0^{\rm jet}$ is not high enough to allow—in the UV-x-ray band—sizable ALP-induced effects on photon polarization for an ALP mass $m_a=10^{-10}$ eV. We assume an initial degree of linear polarization $\Pi_{L,0}=0.3$ in the whole UV-x-ray band and for both the leptonic and the hadronic scenarios according to [118].

In Fig. 20, we report $P_{\gamma\to\gamma}$, and the corresponding final Π_L and χ for both the leptonic and the hadronic cases. What is evident is that the two scenarios are very similar and we observe a little variation only for $E_0\gtrsim5$ keV. The reason for this behavior is as follows. Since the value of the central $B_0^{\rm jet}$ is very low as compared to all other considered cases, we see that the ALP-induced effects are negligible inside the jet. We can observe photon-ALP oscillation effects in the jet for $E_0\gtrsim5$ keV only in the hadronic case because of the higher value of the central $B_0^{\rm jet}$. ALP-induced effects on photon polarization are therefore dominated by the photon-ALP oscillations in the extragalactic space and in the Milky Way. This fact explains why the leptonic and hadronic scenarios are so similar. In the UV-x-ray band the photon-ALP beam propagates in the weak mixing regime, so that all quantities in Fig. 20 and, in particular, the final Π_L—which is strongly modified with respect to $\Pi_{L,0}$—are energy dependent. The binned data in Fig. 20 show low error bars since the pseudo-oscillatory behavior is moderately variable.

The behavior of f_Π in Fig. 21 confirms that the leptonic and hadronic scenarios are very similar. For the benchmark energy $E_0=1$ keV we find a large broadening of the initial $\Pi_{L,0}=0.3$, but the most probable final Π_L remains $\Pi_L=0.3$. Instead, for $E_0=10$ keV we observe that the most probable final Π_L is $\Pi_L>0.8$ with large broadening.

Because conventional physics cannot predict a final $\Pi_L>0.8$, 1ES 0229 + 200 appears as a favored observational target for studies concerning ALP-induced effects on photon polarization for observatories such as IXPE [50], eXTP [51], XL-Calibur [52], NGXP [53] and XPP [54] especially for $E_0\gtrsim5$ keV.

E. Discussion of the polarization detectability

As argued above, OJ 287 and BL Lacertae appear as good observational targets for studies concerning ALP effects on photon polarization both in the x-ray and in the HE band, since we have found that the most probable value

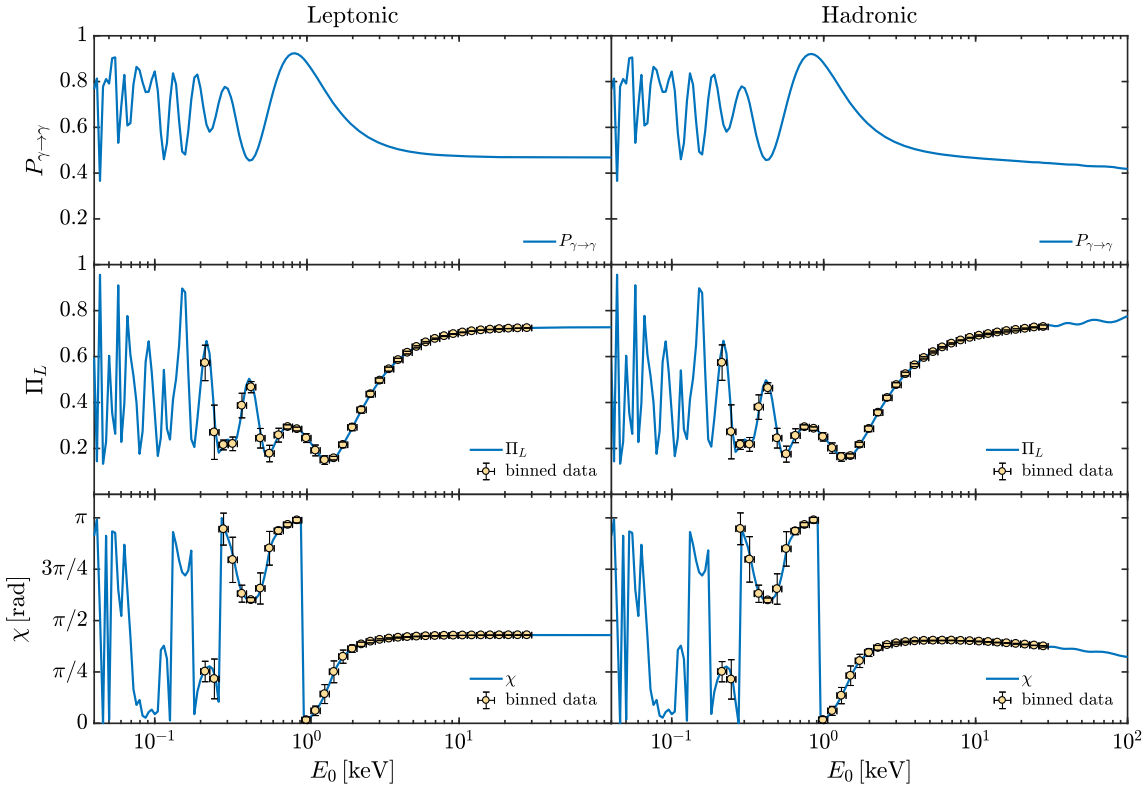

FIG. 20. 1ES 0229 + 200: photon survival probability $P_{\gamma\to\gamma}$ (upper panels), corresponding final degree of linear polarization Π_L (central panels) and final polarization angle χ (lower panels) in the energy range $(4\times10^{-2}$–$10^{2})$ keV. We take $g_{a\gamma\gamma} = 0.5\times10^{-11}$ GeV^{-1}, $m_a \lesssim 10^{-14}$ eV. We consider a leptonic and hadronic emission mechanism in the left and right column, respectively. The initial degree of linear polarization is $\Pi_{L,0} = 0.3$ both in the leptonic and hadronic cases.

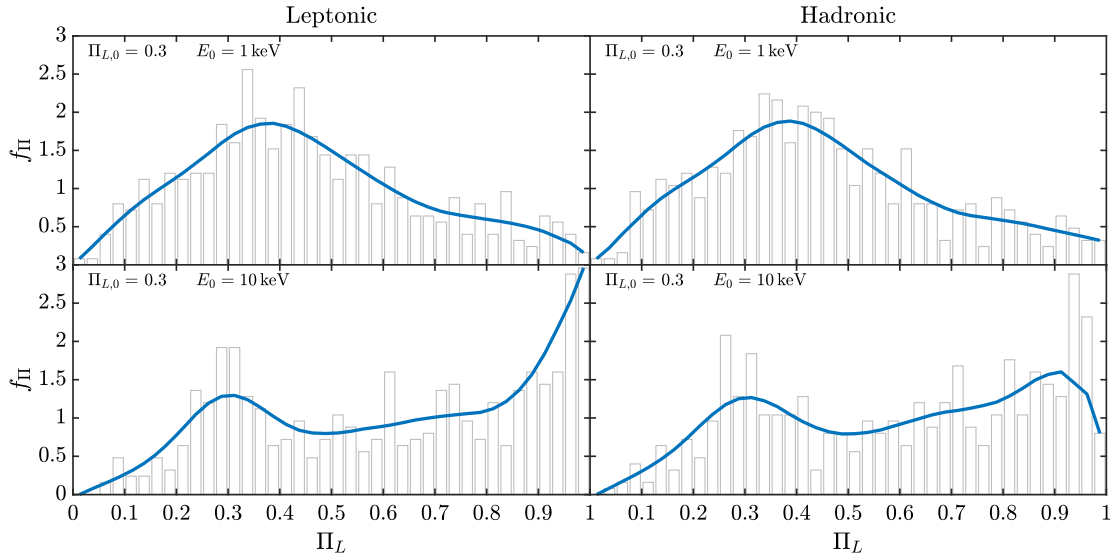

FIG. 21. 1ES 0229 + 200: probability density function f_Π obtained by interpolating the plotted histogram for the final degree of linear polarization Π_L at 1 keV (upper panels) and 10 keV (lower panels) by considering the system in Fig. 20. We consider a leptonic and hadronic emission mechanism in the left and right column, respectively. The initial degree of linear polarization is $\Pi_{L,0} = 0.3$ both in the leptonic and hadronic cases.

for the final Π_L turns out to be $\Pi_L \gtrsim 0.8$ in some cases, a value which cannot be attained even for the hadronic emission mechanism, as shown in Fig. 1 (see also discussion in Sec. IV). Because of the low flux in the HE band, 1ES 0229 + 200 is a good candidate for ALP studies in the x-ray range only. Instead, Markarian 501—which cannot be considered in the HE range owing to the same reason of 1ES 0229 + 200—turns out not to be a good observational target even in the x-ray band owing to its proximity to the Earth and to its low central jet magnetic field.

We have also investigated the relevance of photon-ALP oscillations in the extragalactic space. While $B_{\rm ext} = 1$ nG appears as the most realistic value (see Sec. III D), we have explored also the case $B_{\rm ext} < 10^{-15}$ G which leads to a negligible photon-ALP interaction.

Actually, when $m_a \lesssim 10^{-14}$ eV photon-ALP oscillations in the extragalactic space are effective for $B_{\rm ext} = 1$ nG. A $B_{\rm ext} < 10^{-15}$ G—leading to inefficient photon-ALP oscillations—produces a decrease in the width of the broadening of f_Π in the previous figures. Such an effect is lower in the case of Markarian 501 since it is very close to us. We only note some sizable modification in the behavior of f_Π for 1ES 0229 + 200 at 10 keV. Specifically, high values of f_Π are not anymore the most probable ones when $B_{\rm ext} < 10^{-15}$ G since then photon-ALP oscillations in the jet of 1ES 0229 + 200 are not as strong as in any other considered BL Lac for the low value of its central $B_0^{\rm jet}$.

Instead, when $m_a = 10^{-10}$ eV photon-ALP oscillations in the extragalactic space are not very efficient even for $B_{\rm ext} =$ 1 nG especially in the UV-x-ray band, and so our results remain substantial unchanged by assuming $B_{\rm ext} < 10^{-15}$ G.

The contribution of photon-ALP oscillations in the jet depends on the behavior of $\mathbf{B}_0^{\rm jet}$. In the case of a high $B_0^{\rm jet}$ they produce a substantial effect, while their contribution decreases with a lower $B_0^{\rm jet}$. The effect of the photon-ALP interaction in other crossed regions is less important.

In the present analysis we have considered two choices for the ALP parameter space $(m_a, g_{a\gamma\gamma})$: (i) $m_a \lesssim 10^{-14}$ eV, $g_{a\gamma\gamma} = 0.5 \times 10^{-11}$ GeV^{-1}; and (ii) $m_a = 10^{-10}$ eV, $g_{a\gamma\gamma} = 0.5 \times 10^{-11}$ GeV^{-1}. Both of them are within the CAST bound [64]. However, some new studies about photon-ALP conversion inside galaxy clusters suggest that the case $m_a \lesssim 10^{-14}$ eV, $g_{a\gamma\gamma} = 0.5 \times 10^{-11}$ GeV^{-1} is disfavored with respect to the case $m_a = 10^{-10}$ eV, $g_{a\gamma\gamma} = 0.5 \times 10^{-11}$ GeV^{-1}, as shown in [71–74].

In a previous paper concerning ALP effects on photon polarization in galaxy clusters [49] we have concluded that the HE range represents the best option for such studies, since the parameter choice $m_a \lesssim 10^{-14}$ eV, $g_{a\gamma\gamma} = 0.5 \times 10^{-11}$ GeV^{-1}—disfavored by the latter bounds [71–74]—is the only one producing effects in the x-ray band. However, this conclusion does not apply here for two reasons. First, we observe ALP effects in the x-ray band also in the case $m_a = 10^{-10}$ eV, $g_{a\gamma\gamma} = 0.5 \times 10^{-11}$ GeV^{-1} in the hadronic emission mechanism for OJ 287 and BL Lacertae. Second, the bounds [71–74] are derived by considering galaxy clusters for particular choices of the cluster magnetic field $\mathbf{B}^{\rm clu}$ morphology. If the $\mathbf{B}^{\rm clu}$ configuration is such that the photon-ALP conversion is extremely inefficient, we could observe no effects due to the unfavorable $\mathbf{B}^{\rm clu}$ morphology, instead of concluding that the case $m_a \lesssim 10^{-14}$ eV, $g_{a\gamma\gamma} = 0.5 \times 10^{-11}$ GeV^{-1} should be rejected. Therefore, since in the present situation we are dealing with sources different from those considered in [71–74], we can neither exclude nor consider as disfavored even the case $m_a \lesssim 10^{-14}$ eV, $g_{a\gamma\gamma} = 0.5 \times 10^{-11}$ GeV^{-1}.

As a result, we expect ALP-induced polarization effects both in the x-ray band and in the HE range, which can be detectable by observatories such as IXPE [50], eXTP [51], XL-Calibur [52], NGXP [53], XPP [54] and COSI [55], e-ASTROGAM [56,57], AMEGO [58], respectively. In addition, we want to stress that many other possibilities about the choice of the ALP parameter space $(m_a, g_{a\gamma\gamma})$ can be explored, but they produce final results similar to those arising from our benchmark values.

V. CONCLUSIONS

In this paper, we have investigated the ALP-induced effects on the final degree of linear polarization Π_L and on the polarization angle χ, and we have analyzed the probability density function f_Π of Π_L associated with several realizations of the photon-ALP beam propagation process for photons emitted at the jet base of a few BL Lacs: OJ 287, BL Lacertae, Markarian 501 and 1ES 0229 + 200. We have used the state-of-the-art knowledge about the astrophysical parameters of the media (blazar jet, host galaxy, extragalactic space, Milky Way) crossed by the photon-ALP beam and realistic values of the initial degree of linear polarization $\Pi_{L,0}$. In addition, we have considered both the leptonic and the hadronic emission mechanisms. By specializing the procedure developed in [48] for generic blazars, we have analyzed two different choices for the ALP parameter space: (i) $m_a \lesssim 10^{-14}$ eV, $g_{a\gamma\gamma} = 0.5 \times 10^{-11}$ GeV^{-1}; and (ii) $m_a = 10^{-10}$ eV, $g_{a\gamma\gamma} = 0.5 \times 10^{-11}$ GeV^{-1}. These choices are within the CAST bound [64]. Our results can be detected by IXPE [50], eXTP [51], XL-Calibur [52], NGXP [53] and XPP [54] in the x-ray band, and by COSI [55], e-ASTROGAM [56,57] and AMEGO [58] in the HE range. Our findings can be summarized as follows.

(i) In the x-ray band, the major effects are produced in the case $m_a \lesssim 10^{-14}$ eV, $g_{a\gamma\gamma} = 0.5 \times 10^{-11}$ GeV^{-1}. In particular, OJ 287 and BL Lacertae show a broadening of the initial $\Pi_{L,0}$, while 1ES 0229 + 200 represents a very good observational target since its most probable value for the final Π_L is $\Pi_L > 0.8$ at $E_0 = 10$ keV. The latter value cannot be explained within conventional physics, and so a detection would represent an

additional hint at the ALP existence. We have no sizable difference between leptonic and hadronic emission models for 1ES 0229 + 200. In the case $m_a = 10^{-10}$ eV, $g_{a\gamma\gamma} = 0.5 \times 10^{-11}$ GeV^{-1}, the photon-ALP conversion is inefficient and negligible in all crossed media apart from the blazar jet, provided that hadronic models with a high central magnetic field $B_0^{\rm jet}$ are considered. Accordingly, we observe a dimming of the initial $\Pi_{L,0}$ concerning OJ 287 and BL Lacertae. In all the other situations, the photon-ALP interaction is so inefficient that we observe neither effects on nor modifications of the initial $\Pi_{L,0}$.

(ii) In the HE range, we find strong signals of ALP-induced effects on Π_L and χ in both cases $m_a \lesssim 10^{-14}$ eV, $g_{a\gamma\gamma} = 0.5 \times 10^{-11}$ GeV^{-1} and $m_a = 10^{-10}$ eV, $g_{a\gamma\gamma} = 0.5 \times 10^{-11}$ GeV^{-1}, and for both the leptonic and the hadronic emission mechanisms. Here, we propose OJ 287 and BL Lacertae as good observational targets for ALP studies concerning polarization. In particular, the most probable value for the final Π_L is $\Pi_L \gtrsim 0.8$ especially around 3 MeV. As discussed above, the detection of such a high value of the final Π_L would be a strong indication in favor of the ALP existence, since conventional physics cannot explain it.

Instead, Markarian 501 turns out not to be a good observational target for studies about ALP-induced polarization effects, as explained in Sec. IV C.

Both the two considered choices of the ALP parameters are promising and the case $m_a \lesssim 10^{-14}$ eV, $g_{a\gamma\gamma} = 0.5 \times 10^{-11}$ GeV^{-1} cannot *a priori* be excluded, as explained in Sec. IV E.

Lorentz invariance violation (LIV) can produce a variation in the final Π_L but in terms of a *decrease* of the initial $\Pi_{L,0}$ only [121]. Thus, in all cases where the polarization gets increased with respect to conventional physics, the explanation can only be due to the photon-ALP interaction.

Complementary tests on ALPs similar to those considered in this paper can be performed by the new generation of VHE gamma-ray observatories like ASTRI [122], CTA [123], GAMMA-400 [124], HAWC [125], HERD [126], LHAASO [127] and TAIGA-HiSCORE [128]. Moreover, laboratory experiments like the upgrade of ALPS II at DESY [129], the planned IAXO [130,131] and STAX [132] and the techniques developed by Avignone and collaborators [133–135] can detect them. As stressed in Sec. I, ALPs are very good candidates for the dark matter and if the bulk of the dark matter is indeed made by ALPs they can also be detected by the planned ABRACADABRA experiment [136].

ACKNOWLEDGMENTS

We thank Enrico Costa for discussions. G. G. acknowledges a contribution from the grant ASI-INAF 2015-023-R.1. M. R. acknowledges the financial support by an INFN grant. This work was made possible also by the funding by the INAF Mini Grant "High-energy astrophysics and axionlike particles," PI: Giorgio Galanti.

[1] E. Witten, Phys. Lett. **149B**, 351 (1984).
[2] J. P. Conlon, J. High Energy Phys. 05 (2006) 078.
[3] P. Svrcek and E. Witten, J. High Energy Phys. 06 (2006) 051.
[4] J. P. Conlon, Phys. Rev. Lett. **97**, 261802 (2006).
[5] K.-S. Choi, I.-W. Kim, and J. E. Kim, J. High Energy Phys. 03 (2007) 116.
[6] A. Arvanitaki, S. Dimopoulos, S. Dubovsky, N. Kaloper, and J. March-Russell, Phys. Rev. D **81**, 123530 (2010).
[7] B. S. Acharya, K. Bobkov, and P. Kumar, J. High Energy Phys. 11 (2010) 105.
[8] M. Cicoli, M. Goodsell, and A. Ringwald, J. High Energy Phys. 10 (2012) 146.
[9] A. Cisterna, M. Hassaine, J. Oliva, and M. Rinaldi, Phys. Rev. D **96**, 124033 (2017).
[10] A. Cisterna, C. Erices, X.-M. Kuang, and M. Rinaldi, Phys. Rev. D **97**, 124052 (2018).
[11] J. Jaeckel and A. Ringwald, Annu. Rev. Nucl. Part. Sci. **60**, 405 (2010).
[12] A. Ringwald, Phys. Dark Universe **1**, 116 (2012).
[13] J. Preskill, M. B. Wise, and F. Wilczek, Phys. Lett. **120B**, 127 (1983).
[14] L. F. Abbott and P. Sikivie, Phys. Lett. **120B**, 133 (1983).
[15] M. Dine and W Fischler, Phys. Lett. **120B**, 137 (1983).
[16] P. Arias, D. D Sokoloff, and J. W. F Valle, J. Cosmol. Astropart. Phys. 06 (2012) 008.
[17] G. Alonso-Álvarez, R. S. Gupta, J. Jaekel, and M. Spannowsky, J. Cosmol. Astropart. Phys. 03 (2020) 052.
[18] J. H. Kim, Phys. Rep. **150**, 1 (1987).
[19] H. Y. Cheng, Phys. Rep. **158**, 1 (1988).
[20] J. E. Kim and G. Carosi, Rev. Mod. Phys. **82**, 557 (2010).
[21] D. J. E. Marsch, Phys. Rep. **643**, 1 (2016).
[22] G. G. Raffelt and L. Stodolsky, Phys. Rev. D **37**, 1237 (1988).
[23] L. Maiani, R. Petronzio, and E. Zavattini, Phys. Lett. B **175**, 359 (1986).
[24] I. G. Irastorza and J. Redondo, Prog. Part. Nucl. Phys. **102**, 89 (2018).
[25] G. Galanti, Frascati Phys. Ser. **69**, 101 (2019), http://www.lnf.infn.it/sis/frascatiseries/Volume69/Volume69.pdf.
[26] G. Galanti and M. Roncadelli, Universe **8**, 253 (2022).
[27] F. Tavecchio, M. Roncadelli, G. Galanti, and G. Bonnoli, Phys. Rev. D **86**, 085036 (2012).
[28] G. Galanti, M. Roncadelli, A. De Angelis, and G. F. Bignami, Mon. Not. R. Astron. Soc. **493**, 1553 (2020).

[29] A. De Angelis, M. Roncadelli, and O. Mansutti, Phys. Rev. D **76**, 121301 (2007).
[30] A. De Angelis, G. Galanti, and M. Roncadelli, Phys. Rev. D **84**, 105030 (2011); **87**, 109903(E) (2013).
[31] A. De Angelis, O. Mansutti, and M. Roncadelli, Phys. Lett. B **659**, 847 (2008).
[32] D. Wouters and P. Brun, Phys. Rev. D **86**, 043005 (2012).
[33] G. Galanti and M. Roncadelli, arXiv:1305.2114.
[34] G. Galanti and M. Roncadelli, J. High Energy Astrophys. **20**, 1 (2018).
[35] G. Galanti, F. Tavecchio, M. Roncadelli, and C. Evoli, Mon. Not. R. Astron. Soc. **487**, 123 (2019).
[36] G. Galanti, F. Tavecchio, and M. Landoni, Mon. Not. R. Astron. Soc. **491**, 5268 (2020).
[37] LHAASO Collaboration, GCN Circular n. 32677 (2022), https://gcn.gsfc.nasa.gov/gcn3/32677.gcn3.
[38] Carpet-2 Collaboration, ATel #15669 (2022), https://astronomerstelegram.org/?read=15669.
[39] G. Galanti, L. Nava, M. Roncadelli, F. Tavecchio, and G. Bonnoli, arXiv:2210.05659.
[40] N. Bassan, A. Mirizzi, and M. Roncadelli, J. Cosmol. Astropart. Phys. 05 (2010) 010.
[41] P. Jain, S. Panda, and S. Sarala, Phys. Rev. D **66**, 085007 (2002).
[42] N. Agarwal, A. Kamal, and P. Jain, Phys. Rev. D **83**, 065014 (2011).
[43] A. Payez, J. R. Cudell, and D. Hutsemékers, Phys. Rev. D **84**, 085029 (2011).
[44] N. Agarwal, P. K. Aluri, P. Jain, P. K. Aluri, P. Jain, U. Khanna, and P. Tiwari, Eur. Phys. J. C **72**, 1928 (2012).
[45] R. Perna, W. C. G. Ho, L. Verde, M. van Adelsberg, and R. Jimenez, Astrophys. J. **748**, 116 (2012).
[46] F. Day and S. Krippendorf, Galaxies **6**, 45 (2018).
[47] G. Galanti, Phys. Rev. D **105**, 083022 (2022).
[48] G. Galanti, Phys. Rev. D **107**, 043006 (2023).
[49] G. Galanti, M. Roncadelli, F. Tavecchio, and E. Costa, Phys. Rev. D **107**, 103007 (2023).
[50] M. Weisskopf *et al.*, J. Astron. Telesc. Instrum. Syst. **8**, 026002 (2022).
[51] S. N. Zhang *et al.*, Sci. China Phys. Mech. Astron. **62**, 29502 (2019).
[52] Q. Abarr *et al.*, Astropart. Phys. **126**, 102529 (2021).
[53] P. Soffitta *et al.*, Exp. Astron. **51**, 1109 (2021).
[54] K. Jahoda *et al.*, arXiv:1907.10190.
[55] C.-Y. Yang *et al.*, Proc. SPIE Int. Soc. Opt. Eng. **10699**, 642 (2018), https://www.spiedigitallibrary.org/conference-proceedings-of-spie/10699/2312556/The-polarimetric-performance-of-the-Compton-spectrometer-and-imager-COSI/10.1117/12.2312556.full.
[56] A. De Angelis *et al.* (e-ASTROGAM Collaboration), Exp. Astron. **44**, 25 (2017).
[57] V. Tatischeff *et al.* (e-ASTROGAM Collaboration), Proc. SPIE Int. Soc. Opt. Eng. **10699**, 106992J (2018).
[58] C. A. Kierans (AMEGO Collaboration), Proc. SPIE Int. Soc. Opt. Eng. **11444**, 1144431 (2020).
[59] W. Heisenberg and H. Euler, Z. Phys. **98**, 714 (1936).
[60] V. S. Weisskopf, K. Dan. Vidensk. Selsk. Mat. Fys. Medd. **14**, 6 (1936).
[61] J. Schwinger, Phys. Rev. **82**, 664 (1951).
[62] G. Galanti and M. Roncadelli, Phys. Rev. D **98**, 043018 (2018).
[63] A. Dobrynina, A. Kartavtsev, and G. Raffelt, Phys. Rev. D **91**, 083003 (2015); **91**, 109902(E) (2015).
[64] CAST Collaboration, Nat. Phys. **13**, 584 (2017).
[65] A. Ayala, I. Domínguez, M. Giannotti, A. Mirizzi, and O. Straniero, Phys. Rev. Lett. **113**, 191302 (2014).
[66] A. Payez, C. Evoli, T. Fischer, M. Giannotti, A. Mirizzi, and A. Ringwald, J. Cosmol. Astropart. Phys. 02 (2015) 006.
[67] M. Ajello *et al.* (Fermi-LAT Collaboration), Phys. Rev. Lett. **116**, 161101 (2016).
[68] M. Berg, J. P. Conlon, F. Day, N. Jennings, S. Krippendorf, A. J. Powell, and M. Rummel, Astrophys. J. **847**, 101 (2017).
[69] J. P. Conlon, F. Day, N. Jennings, S. Krippendorf, and M. Rummel, J. Cosmol. Astropart. Phys. 07 (2017) 005.
[70] M. Meyer and T. Petrushevska, Phys. Rev. Lett. **124**, 231101 (2020); **125**, 119901(E) (2020).
[71] C. S. Reynolds, M. C. D. Marsh, H. R. Russell, A. C. Fabian, R. Smith, F. Tombesi, and S. Veilleux, Astrophys. J. **890**, 59 (2020).
[72] J. Sisk-Reynés *et al.*, Mon. Not. R. Astron. Soc. **510**, 1264 (2022).
[73] S. Schallmoser, S. Krippendorf, F. Chadha-Day, and J. Weller, Mon. Not. R. Astron. Soc. **514**, 329 (2022).
[74] J. H. Matthews, C. S. Reynolds, M. C. D. Marsh, J. Sisk-Reynés, and P. E. Rodman, Astrophys. J. **930**, 90 (2022).
[75] C. Dessert, D. Dunsky, and B. R. Safdi, Phys. Rev. D **105**, 103034 (2022).
[76] A. Kosowsky, Ann. Phys. (N.Y.) **246**, 49 (1996).
[77] G. B. Rybicki and A. P. Lightman, *Radiative Processes in Astrophysics* (Wiley, New York, 1979).
[78] The quantities E_L and E_H are derived for the case of: (i) fully polarized photons, (ii) no photon absorption, (iii) homogeneous medium, and (iv) constant **B** field. The general case is totally similar but the analytic expressions of E_L and E_H are cumbersome and shed no light on the behavior of the system. This is the reason why we report the simplified case here. Yet, in our calculations the fully accurate system is considered.
[79] M. C. Begelman, R. D. Blandford, and M. J. Rees, Rev. Mod. Phys. **56**, 255 (1984).
[80] G. Ghisellini and F. Tavecchio, Mon. Not. R. Astron. Soc. **397**, 985 (2009).
[81] R. E. Pudritz, M. J. Hardcastle, and D. C. Gabuzda, Space Sci. Rev. **169**, 27 (2012).
[82] F. Tavecchio, G. Ghisellini, G. Ghirlanda, L. Foschini, and L. Maraschi, Mon. Not. R. Astron. Soc. **401**, 1570 (2010).
[83] L. Maraschi, G. Ghisellini, and A. Celotti, Astrophys. J. Lett. **397**, L5 (1992).
[84] M. Sikora, M. C. Begelman, and M. J. Rees, Astrophys. J. **421**, 153 (1994).
[85] S. D. Bloom and A. P. Marscher, Astrophys. J. **461**, 657 (1996).
[86] K. Mannheim, Phys. Rev. D **48**, 2408 (1993).
[87] K. Mannheim, Astron. Astrophys. **269**, 67 (1993), https://articles.adsabs.harvard.edu/pdf/1993A%26A...269...67M.

[88] A. Mücke, R. J. Protheroe, R. Engel, J. P. Rachen, and T. Stanev, Astropart. Phys. **18**, 593 (2003).
[89] F. Tavecchio, M. Roncadelli, and G. Galanti, Phys. Lett. B **744**, 375 (2015).
[90] D. Moss D. and A. Shukurov, Mon. Not. R. Astron. Soc. **279**, 229 (1996).
[91] A. Franceschini and G. Rodighiero, Astron. Astrophys. **603**, A34 (2017).
[92] A. De Angelis, G. Galanti, and M. Roncadelli, Mon. Not. R. Astron. Soc. **432**, 3245 (2013).
[93] G. Galanti, F. Piccinini, M. Roncadelli, and F. Tavecchio, Phys. Rev. D **102**, 123004 (2020).
[94] A. Saldana-Lopez, A. Domínguez, P. G. Pérez-González, J. Finke, M. Ajello, J. R. Primack, V. S. Paliya, and A. Desai, Mon. Not. R. Astron. Soc. **507**, 5144 (2021).
[95] A. Neronov and I. Vovk, Science **328**, 73 (2010).
[96] R. Durrer and A. Neronov, Astron. Astrophys. Rev. **21**, 62 (2013).
[97] M. S. Pshirkov, P. G. Tinyakov, and F. R. Urban, Phys. Rev. Lett. **116**, 191302 (2016).
[98] P. P. Kronberg, Rep. Prog. Phys. **57**, 325 (1994).
[99] D. Grasso and H. R. Rubinstein, Phys. Rep. **348**, 163 (2001).
[100] M. J. Rees and G. Setti, Nature (London) **219**, 127 (1968).
[101] F. Hoyle, Nature (London) **223**, 936 (1969).
[102] P. P. Kronberg, H. Lesch, and U. Hopp, Astrophys. J. **511**, 56 (1999).
[103] S. Furlanetto and A. Loeb, Astrophys. J. **556**, 619 (2001).
[104] J. M. Yao, R. N. Manchester, and N. Wang, Astrophys. J. **835**, 29 (2017).
[105] R. Jansson and G. R. Farrar, Astrophys. J. **757**, 14 (2012).
[106] R. Jansson and G. R. Farrar, Astrophys. J. **761**, L11 (2012).
[107] M. C. Beck, A. M. Beck, R. Beck, K. Dolag, A. W. Strong, and P. Nielaba, J. Cosmol. Astropart. Phys. 05 (2016) 056.
[108] M. S. Pshirkov, P. G. Tinyakov, P. P. Kronberg, and K. J. Newton-McGee, Astrophys. J. **738**, 192 (2011).
[109] The polarization features cannot be washed out by the blazar variability, as the ALP effects are independent on the blazar state, as they depend only on the magnetization and absorption properties of the crossed media.
[110] H. Zhang and M. Böttcher, Astrophys. J. **774**, 18 (2013).
[111] L. Di Gesu *et al.*, Astrophys. J. Lett. **938**, L7 (2022).
[112] I. Liodakis *et al.*, Nature (London) **611**, 677 (2022).
[113] R. Middei *et al.*, Astrophys. J. Lett. **953**, L28 (2023).
[114] D. N. Burrows *et al.*, Space Sci. Rev. **120**, 165 (2005).
[115] Our goal is to provide an idea of what an observer may expect, so that the central values of the data points are computed by averaging the sampled calculation points within the bin and the uncertainties are calculated by evaluating the standard deviation. In particular—for each bin—we bin our theoretical results concerning the Stokes parameters by collecting all the theoretical data within the bin width and we calculate its mean μ and variance σ with no weighting procedure for the heuristic nature of our evaluation. We then employ the standard theory of error propagation to obtain the error bars of the derived quantities Π_L and χ. See also [49] for the complete description of the assumed binning procedure.
[116] M. Böttcher, A. Reimer, K. Sweeney, and A. Prakash, Astrophys. J. **768**, 54 (2013).
[117] F. Tavecchio *et al.*, Astrophys. J. **554**, 725 (2001).
[118] F. Tavecchio, M. Landoni, L. Sironi, and P. Coppi, Mon. Not. R. Astron. Soc. **480**, 2872 (2018).
[119] G. Bonnoli, F. Tavecchio, G. Ghisellini, and T. Sbarrato, Mon. Not. R. Astron. Soc. **451**, 611 (2015).
[120] L. Costamante, G. Bonnoli, F. Tavecchio, G. Ghisellini, G. Tagliaferri, and D. Khangulyan, Mon. Not. R. Astron. Soc. **477**, 4257 (2018).
[121] V. A. Kostelecký and M. Mewes, Phys. Rev. D **80**, 015020 (2009).
[122] S. Vercellone *et al.*, J. High Energy Astrophys. **35**, 1 (2022).
[123] https://www.cta-observatory.org/.
[124] A. E. Egorov, N. P. Topchiev, A. M. Galper, O. D. Dalkarov, A. A. Leonov, S. I. Suchkov, and Y. T. Yurkin, J. Cosmol. Astropart. Phys. 11 (2020) 049.
[125] https://www.hawc-observatory.org/.
[126] X. Huang *et al.*, Astropart. Phys. **78**, 35 (2016).
[127] Z. Cao *et al.*, Chin. Phys. C **46**, 035001 (2022).
[128] https://taiga-experiment.info/taiga-hiscore/.
[129] R. Bähre *et al.*, J. Instrum. **8**, T09001 (2013).
[130] I. G. Irastorza *et al.* (IAXO Collaboration), J. Cosmol. Astropart. Phys. 06 (2011) 013.
[131] E. Armengaud *et al.*, J. Cosmol. Astropart. Phys. 06 (2019) 047.
[132] L. M. Capparelli, G. Cavoto, J. Ferretti, F. Giazotto, A. D. Polosa, and P. Spagnolo, Phys. Dark Universe **12**, 37 (2016).
[133] F. T. Avignone III, Phys. Rev. D **79**, 035015 (2009).
[134] F. T. Avignone III, R. J. Crewick, and S. Nussinov, Phys. Lett. B **681**, 122 (2009).
[135] F. T. Avignone III, R. J. Crewick, and S. Nussinov, Astropart. Phys. **34**, 640 (2011).
[136] Y. Kahn, B. R. Safdi, and J. Thaler, Phys. Rev. Lett. **117**, 141801 (2016).